Research and Development Progress Report No. 714 • August 1971
Int-OSW-RDPR-71-714

Model Studies of Outfall Systems For Desalination Plants (Part I — Flume Study)

By F. M. Holly, Jr., and J. L. Grace, Jr., U. S. Army Engineer Waterways Experiment Station, Vicksburg, Mississippi, for Office of Saline Water, J. W. O'Meara, Acting Director; W. F. Savage, Assistant Director, Engineering and Development; W. W. Rinne, Chief, Special Projects Division; C. L. Gransee, Project Engineer.

Contract No. 14-30-2656

United States Department of the Interior • Rogers C. B. Morton, Secretary
James R. Smith, Assistant Secretary, Water and Power Resources

For sale by the Superintendent of Documents, U.S. Government Printing Office
Washington, D.C. 20402 - Price 65 cents
Stock Number 2400-0664

As the Nation's principal conservation agency, the Department of the Interior has basic responsibilities for water, fish, wildlife, mineral, land, park, and recreational resources. Indian Territorial affairs are other major concerns of America's "Department of Natural Resources".

The Department works to assure the wisest choice in managing all our resources so each will make its full contribution to a better United States—now and in the future.

FOREWORD

This is one of a continuing series of reports designed to present accounts of progress in saline water conversion and the economics of its application. Such data are expected to contribute to the long-range development of economical processes applicable to low-cost demineralization of sea and other saline water.

Except for minor editing, the data herein are as contained in a report submitted by the contractor. The data and conclusions given in the report are essentially those of the contractor and are not necessarily endorsed by the Department of the Interior.

PREFACE

The experimental investigation reported herein was conducted under Contract 14-30-2656 between the U. S. Department of the Interior and the U. S. Army Corps of Engineers. The study was conducted in the Hydraulics Division of the U. S. Army Engineer Waterways Experiment Station during the period June 1970 to July 1971 under the direction of Mr. E. P. Fortson and Mr. H. B. Simmons, Chiefs of the Hydraulics Division during this period, and Mr. T. E. Murphy, Chief of the Structures Branch. The tests were conducted by SP5 F. M. Holly, Jr., under the supervision of Mr. J. L. Grace, Jr., Chief of the Spillways and Conduits Section. This report was prepared by Messrs. Holly and Grace.

Messrs. Walter Rinne and C. L. Gransee of the Office of Saline Water, Professor R. O. Reid of Texas A&M University, and Dr. M. A. Zeitoun of Dow Chemical Company visited the Waterways Experiment Station during the investigation phase of the study to observe and discuss testing and the application of results.

COL Ernest D. Peixotto, CE, was Director of the Waterways Experiment Station during the conduct of the investigation and the preparation and publication of this report. Mr. F. R. Brown was Technical Director.

TABLE OF CONTENTS

CONTENTS

LIST OF TABLES

LIST OF FIGURES

CONVERSION FACTORS, BRITISH TO METRIC UNITS OF MEASUREMENT

British units of measurement used in this report can be converted to metric units as follows:

Multiply	By	To Obtain
inches	2.54	centimeters
feet	0.3048	meters
square feet	0.092903	square meters
cubic feet	0.02831685	cubic meters
feet per second	0.3048	meters per second*
cubic feet per second	0.02831685	cubic meters per second
feet per second per second	0.3048	meters per second per second
Fahrenheit degrees	5/9	Celsius or Kelvin degrees**
gallons (U. S.)	3.785412	cubic decimeters
square feet per second	0.0930	square meters per second

* To obtain velocity in knots, multiply velocity in feet per second (fps) by 1.689.

** To obtain Celsius (C) temperature readings from Fahrenheit (F) readings, use the following formula: $C = (5/9)(F - 32)$. To obtain Kelvin (K) readings, use: $K = (5/9)(F - 32) + 273.15$.

SECTION I: INTRODUCTION

A. The Problem and Purpose of Study

In the planning and design of plants for desalination of salt water, a major consideration is the environmentally acceptable disposal of the waste brine--a warm, dense, highly salt-laden effluent whose concentrations of copper and other metallic ions are considered to be a threat to the marine ecology. Among the several alternatives for disposal of this brine is the economically attractive one of discharging the effluent back into the ocean or estuary from which it was withdrawn. However, a means of mixing the dense liquid with the ambient fluid sufficiently to dilute the concentration of various salts to safe levels is required.

The Office of Saline Water has been funding an ongoing research program through the Dow Chemical Company, in which Dr. M. A. Zeitoun of Dow Chemical Company and Professor R. O. Reid of Texas A&M University have been developing conceptual designs of desalination plant outfall systems and numerical models for prediction of their performance. The purpose of the present study was to utilize a physical model to evaluate the degree of mixing attainable through use of a diffuser located on the estuary floor or the ocean floor beyond the surf zone, from which the dense brine is discharged vertically through circular ports into a uniform and steady crosscurrent.

B. Approach and Specific Objectives

Experiments at the U. S. Army Engineer Waterways Experiment Station (WES) were conducted in two areas: (1) tests of multiple-port diffusers in three distorted estuary models, to be reported under separate cover as Part II of this report, and (2) tests of single- and multiple-port diffusers at an undistorted scale of 1:20 in a flume having a level bottom and conveying uniform steady flow. The flume tests reported herein involved a study of the separate effects of the following variables on the distribution of brine downstream from a diffuser:

Variable	Prototype Range
U = ambient velocity	0.1 to 1.0 knot
V_o = port discharge velocity	8 to 20 fps
$\Delta\rho_m$ = density difference between brine and ambient fluid	0.0045 to 0.026 g/cc
D_o = port diameter	3, 6, and 9 in.

Specifically, the objectives were as follows:

1. To evaluate the effects of the above variables on the maximum

height of the upper boundary of an arcing plume, the lateral spread of the plume, and the downstream density distribution.

2. To determine whether single-port results can be superimposed to predict multiple-port mixing.

3. To determine whether or not heated brine has significantly different mixing characteristics as compared with nonheated brine.

4. To evaluate the mixing advantages of a multiple-port diffuser over a simple outfall pipe.

C. Qualitative Description of Jet Plume

While specific characteristics of the dense plumes will be evaluated as part of this report, it appears appropriate at the outset to describe qualitatively the general characteristics of dense jets discharged vertically into uniform ambient flow. At ambient flows only slightly above zero the jet rises nearly vertically in the longitudinal plane, arcing and falling relatively intact. Upon hitting the bottom, the brine forms rings that rapidly expand concentrically upstream and downstream in close proximity to the bottom. The effect appears to be one of gravity waves; any localized buildup of dense liquid on the bottom is unstable and must result in outward spreading to reach equilibrium.

As ambient flow is increased, the gravity wave effect is less dominant; rings form on the bottom and spread rapidly, but tend to move downstream with the ambient flow in distinct waves. At moderate ambient velocities the rings do not appear to form; the plume arcs to a peak, then flows downstream and spreads slightly as it slowly settles to the bottom.

The above discussion is descriptive of totally submerged jets. For cases in which the jet is discharged with sufficient energy to reach the surface, its characteristics are significantly altered. At low ambient velocities the plume boils and spreads concentrically along the surface; highly diluted brine then gradually falls toward the bottom. With higher ambient velocities the jet boils and spreads to an initially lesser degree than it does with low ambient velocities and is swept downstream as it spreads laterally and falls toward the bottom. However, the spread and dilution of a jet that reaches the surface are generally greater than for one totally submerged.

SECTION II: SUMMARY AND CONCLUSIONS

Nearly 400 tests were run in a 1:20-scale, uniform flow flume to evaluate the effects of port diameter, brine flow rate, density differential, and ambient velocity on the geometry and mixing characteristics of a dense jet discharged vertically through a single port. Geometry data were taken through photographic and visual observations; dilution data were compiled using combined conductivity-temperature probes. The product of the ratio of ambient to port velocities and a port densimetric Froude number has been found to be the significant parameter in all aspects of the problem.

The maximum height of the upper boundary of a jet, Z_m, can be predicted with the following equations:

$$\frac{Z_m - D}{D_o} = C\mathbb{F}_D$$

$$C = 3.4 \times 10^{-0.148(U/V_o)\mathbb{F}_D}$$

where

D = outfall diameter, ft

D_o = port diameter, ft

$\mathbb{F}_D$ = port densimetric Froude number

U = ambient velocity, fps

V_o = port velocity, fps

A correlation of the minimum dilution at a downstream station with relevant dimensionless flow parameters provides for prediction of the maximum concentrations to be expected for a given set of design/operating parameters, according to the following equation:

$$\epsilon_m = \left[31 \times 10^{0.4(U/V_o)\mathbb{F}_D}\right]\left(\frac{x}{x_o}\right)^{0.68}$$

where

x = distance downstream from diffuser, ft

x_o = distance at which plume falls to bottom, ft

ϵ_m = minimum observed dilution

Correlations of lateral plume width with downstream distance led to the following equations for prediction of plume spread:

$$\frac{w}{w_o} = \left(\frac{x}{x_o}\right)^R$$

where

w = total plume width, ft

w_o = plume width at $x = x_o$, ft

and

$$R = 3.02 \times 10^{-0.26(U/V_o)\mathbb{F}_D} \quad \text{for} \quad x \le x_o$$

$$R = 0.61 \log_{10}\left(4 \frac{U}{V_o} \mathbb{F}_D\right) \quad \text{for} \quad x > x_o$$

The normalizing quantities x_o and w_o can be predicted by

$$x_o = 9.62\, Z_m \log_{10}\left(2 \frac{U}{V_o} \mathbb{F}_D\right)$$

$$w_o = 1.51\, Z_m \log_{10}\left(4.91 \frac{U}{V_o} \mathbb{F}_D\right)$$

Tests using a multiple-port diffuser verified that linear superposition of single-port results can be used to predict multiple-port mixing characteristics. Tests using heated brine indicated that the presence of a temperature differential of up to 10°C between the brine and ambient fluid has no significant effect on the plume mixing characteristics. A multiple-port diffuser was found to have a significant advantage over a simple outfall pipe in keeping high concentrations of dissolved metallic ions away from the ocean floor.

SECTION III: DESCRIPTION OF TEST FACILITY

A. Flume

In choosing a scale for the laboratory model, it was important to ensure that Reynolds numbers were kept high enough so that the flows could be considered fully turbulent, as in prototype situations. A 1:20 scale of model to prototype was chosen and similitude based upon the Froudian criterion dictates the following correspondence between geometric and kinematic parameters of the two systems:

	Prototype	Model
Length	20	1
Area	400	1
Volume	8000	1
Time	4.4721	1
Velocity	4.4721	1
Discharge	1788.840	1
$\mathbb{R}_p$	1.7×10^5	1.9×10^3
$\mathbb{R}_c$	5.6×10^5	6.3×10^3

where

$$\mathbb{R}_p = \frac{V_o D_o}{\nu} , \quad \mathbb{R}_c = \frac{UH}{\nu}$$

$\mathbb{R}_p$ = port Reynolds number

$\mathbb{R}_c$ = channel Reynolds number

V_o = port discharge velocity

D_o = port diameter

ν = kinematic viscosity of water

U = ambient flow velocity

H = ambient flow depth (40 ft used)

The above Reynolds numbers are representative of the minimum values simulated and indicate that all flow situations investigated were of the fully developed turbulent type. At a scale of 1:20 the model reproduces a section of level ocean floor 140 ft wide and 600 ft long, with a maximum water depth of 40 ft. Figs. 1 and 2 are photographs of the flume. The flume bottom was surrounded by 6- by 6-in. gutters that trapped dense fluid before it reflected off the flume walls. A sump area at the elevation of the gutters and a cutoff wall extending across the downstream end of the flume were built to provide an area from which excess brine could be pumped back into holding tanks. It was found during preliminary testing that it was impractical to reclaim the diluted brine, and the cutoff wall was removed. Water-surface elevations were regulated by means of a downstream gate. One wall of the flume was constructed of transparent plastic (1/2 in. and 3/4 in. thick) mounted in a wooden frame to provide for visual observations of dispersion throughout the full length of the flume. The opposite masonry wall was finished with plaster. The flume bottom was a smooth-troweled concrete slab with two coats of glossy white epoxy paint; 1.0-ft grids were painted on both vertical walls as well as on the bottom of the flume.

The experimental work reported by Dow Chemical Company[1] verified that in modeling a dense discharge it is the density difference between the effluent and the ambient fluid, rather than the overall level of density, which is important. Therefore, the WES flume was provided with a recirculating freshwater system to model the ocean current. Fresh water supplied by pumps and a constant head tank was discharged through either a 20- or a 6-in. supply line into an 8-ft-wide forebay that was separated from the main flume by flow-straightening tiles and a rock baffle. Venturi tubes on the two supply lines provided for accurate measurement of model discharges that ranged from 0.2 to 14 cfs.

B. Brine Supply System

Two 8- by 7- by 3-ft tanks (fig. 2) were used to prepare and store brine solutions; sump pumps on the tank floor kept the solutions well mixed. Two 8-gpm centrifugal pumps with stainless steel rotors pumped from either tank through either of two Rotameters or a 1- by 1/2-in. venturi. A 2- by 2- by 1-ft tank with a point gage attached was used to calibrate volumetrically the venturi and Rotameters for model discharges ranging from 0.00014 to 0.012 cfs. The various calibrations were found to be essentially independent of the small brine density variations expected. All brine piping was 1-in. copper tubing with appropriate reducers for the pumps and Rotameters.

The model diffuser consisted of a length of pipe extending across the full width of the flume at sta 0+00. A threaded connection permitted installation of a number of different diffusers with discharge ports drilled vertically at the flume center line for most cases.

C. Flume Velocity Distribution

Velocity measurements were made in the flume to establish the degree of uniform flow obtained. Fig. 3 is a plot of velocity contours, looking

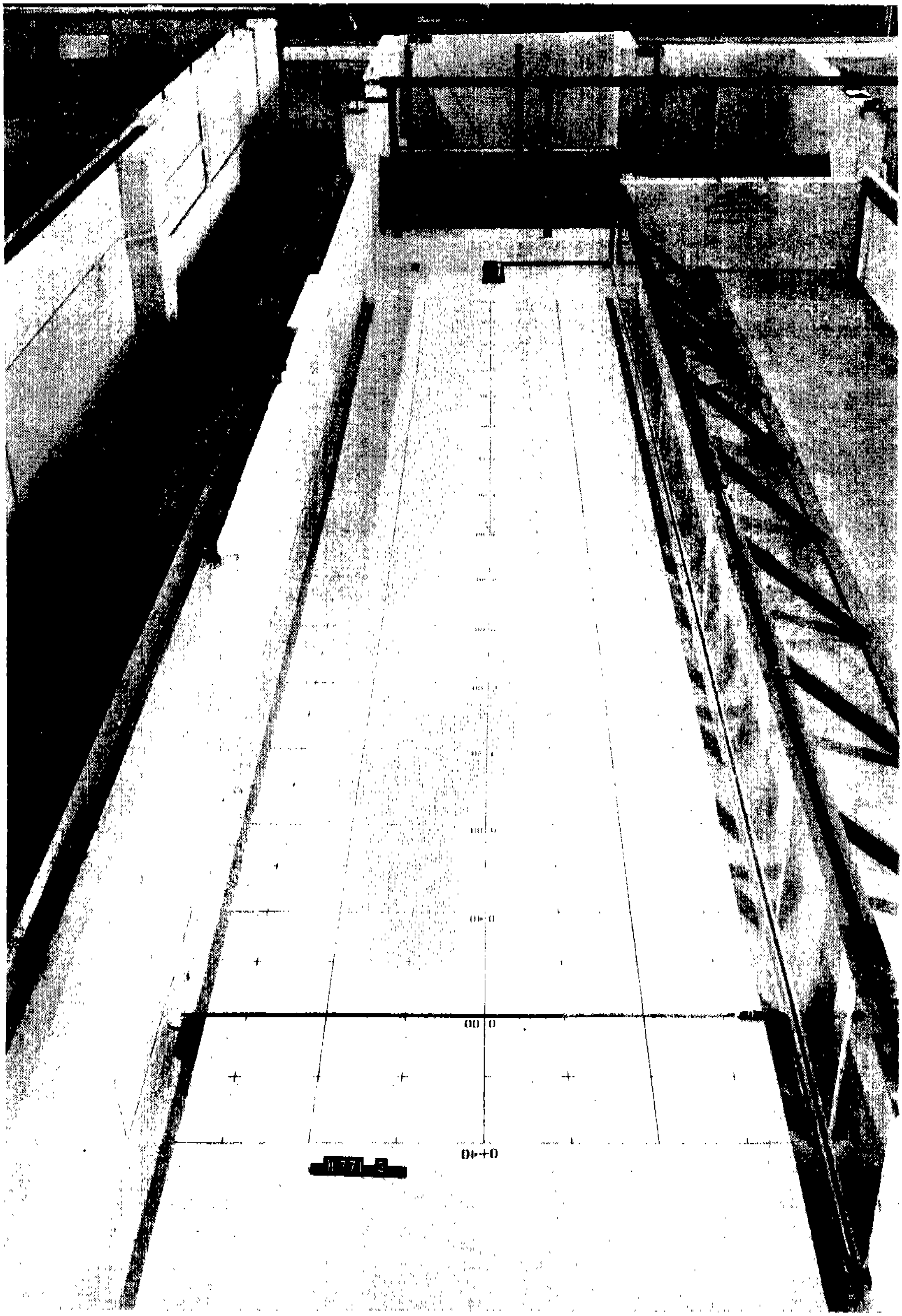

Fig. 1. Uniform flow flume (looking downstream)

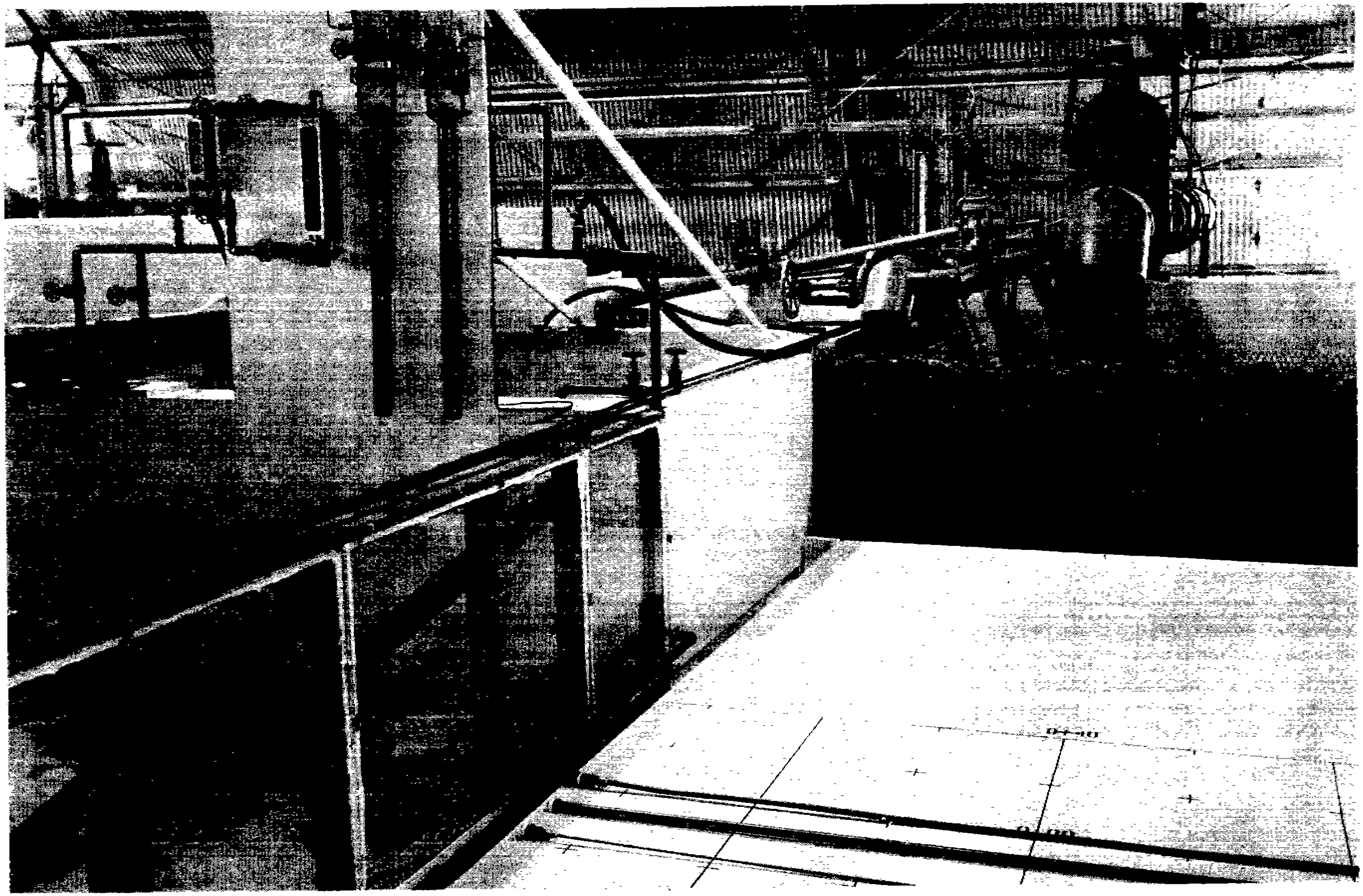

Fig. 2. Flume forebay and brine supply system (looking upstream)

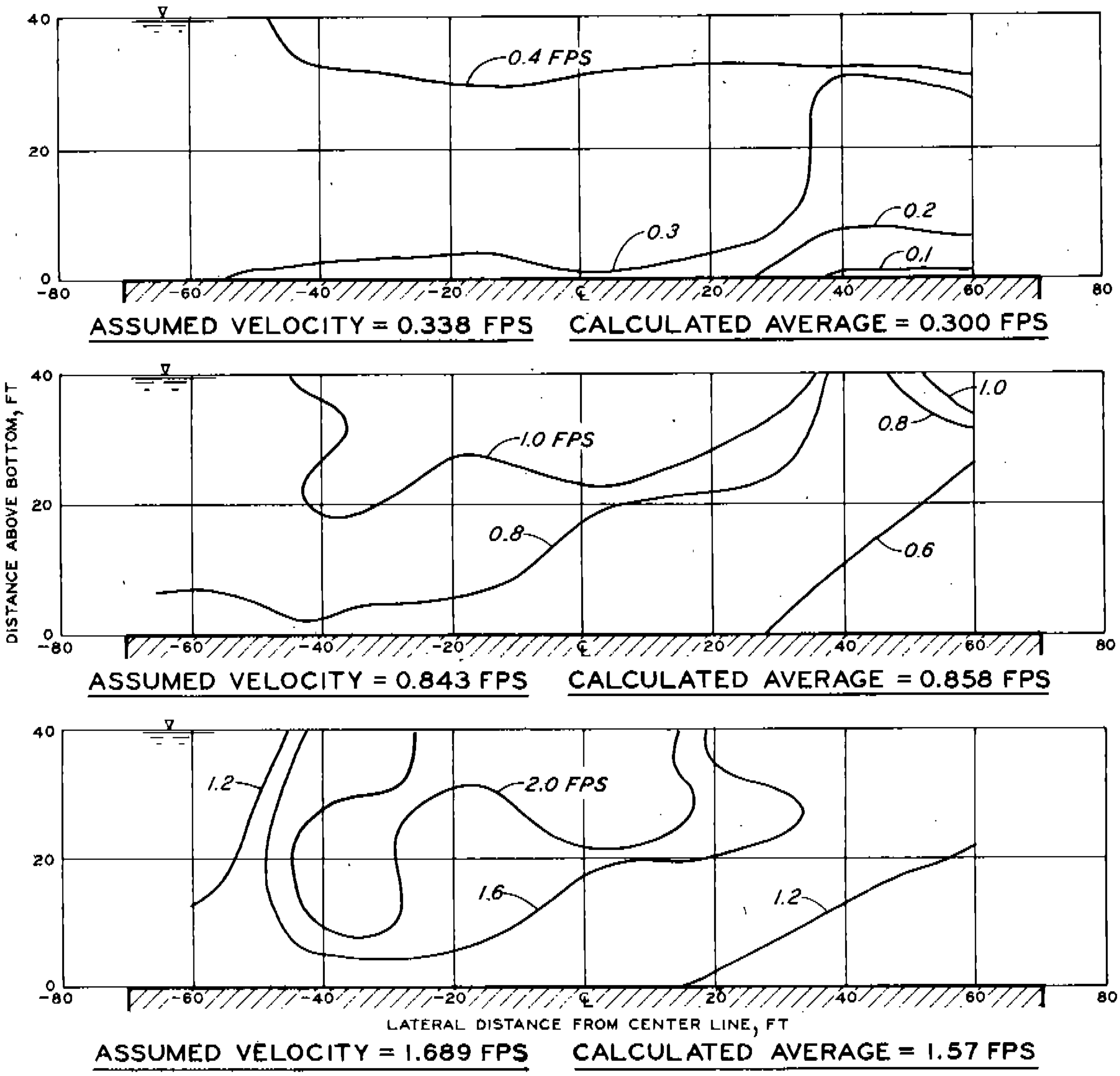

Fig. 3. Prototype velocity contours in flume (looking upstream) at x = -36 ft

upstream, determined at sta 0-36 (prototype) for assumed ambient velocities of 0.2, 0.5, and 1.0 knot (prototype). The irregular rock baffle, along with the nonsymmetrical water-supply situation, is responsible for the nonuniformity of the flow. However, the averaged velocity measurements agree well with the assumed velocities based on a discharge divided by cross-sectional area calculation; the deviations from uniform flow are not considered to be significantly different from what might be expected in a prototype ocean situation.

D. Photograph Provisions

Two 30- by 40-in. mirrors were built into a movable periscope that permitted eye-level observation of tests in the flume. Banks of photoflood lamps were placed over the flume to provide illumination for two 16-mm movie cameras that were used to photograph brine plumes through the periscope and plastic flume wall. A grid of known dimensions was placed vertically on the flume center line and photographed during initial testing for later use in scaling plume tracings.

E. Flume Instrumentation

A conductivity-temperature system was selected for use in quantifying dilution; the in situ probes were considered to have an inherent advantage over fluorescent dye methods, which require removal of a sample from the flow. A Digitec Model 501-N Digital Thermometer, made by the United Systems Corp., was used with remote probes on 50-ft leads to provide digital readout in degrees Centigrade.

The conductivity probes were designed and built at WES. Two copper electrodes were inserted into a plastic block and soldered to wire leads. The leads ran out through a length of rigid plastic tubing, which was attached to the plastic block. The entire assemblage was sealed with epoxy paint with only the electrode tips remaining bare. Each conductivity probe was then inserted into a point gage, and a thermistor probe was taped alongside it. Fig. 4 shows a typical probe assembly, nine of which were placed on rails over the flume for three-dimensional positioning within 1/2 in. of the boundaries.

A Conductivity Meter, Model R13x10-S58-P164K, made by Beckman Instruments, Inc., was used to measure the conductivity of one probe at a time. A constant resistance of 527 ohms was placed across the temperature-compensating circuit of the instrument and a 0-100 thousand ohm potentiometer was added to its bridge circuit so that the conductivity range could be varied. A 0- to 100-mv digital voltmeter and chart recorder were driven by a linearizing circuit in the conductivity meter, providing a linear record of conductivity variations. As testing proceeded it was necessary to add a so-called integrating circuit in which a capacitor accumulates voltage proportional to conductivity so that a time-averaged conductivity could be obtained.

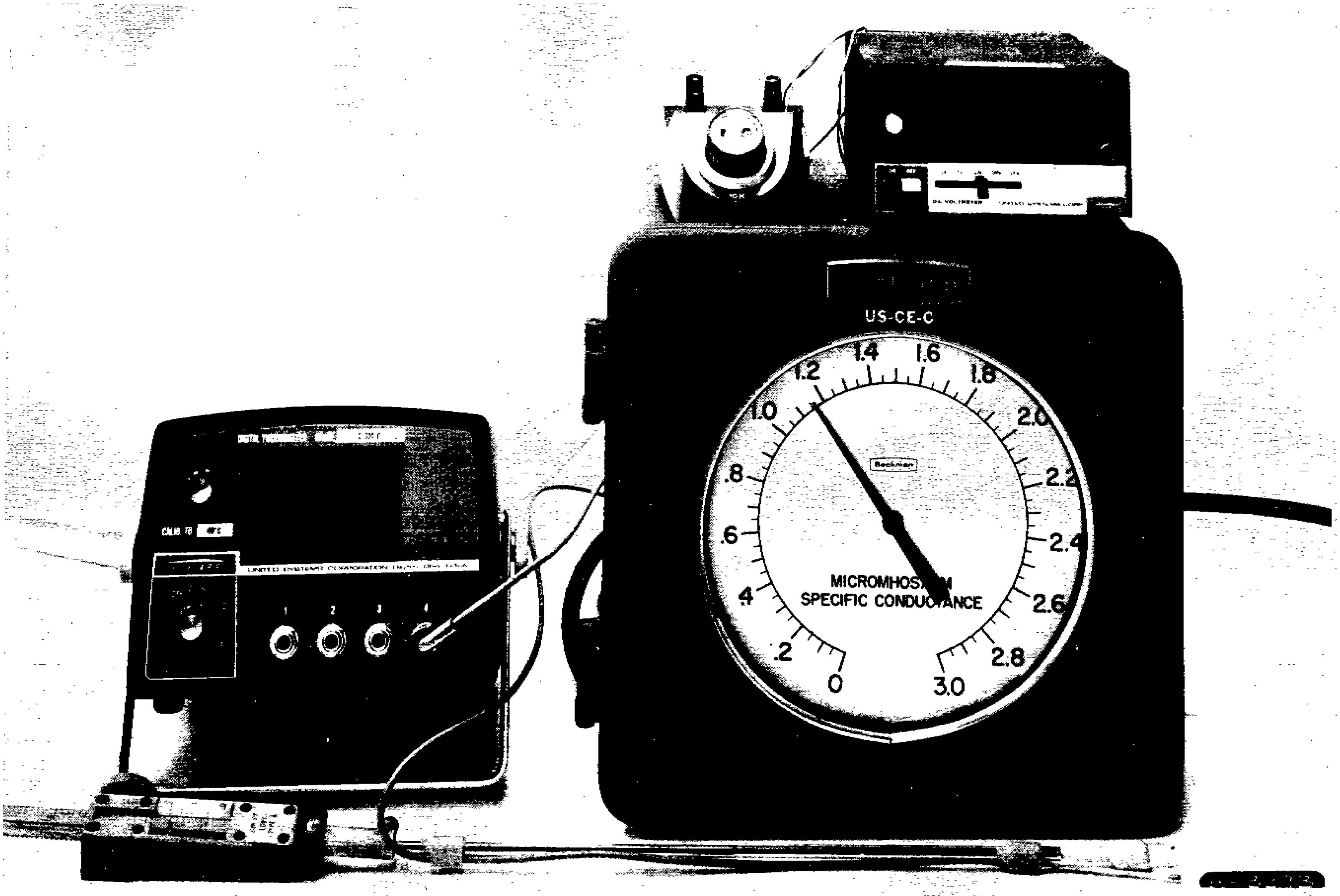

Fig. 4. Conductivity-temperature probe assembly and readout

SECTION IV. PROGRAM AND PROCEDURE OF TESTS

A. General

During preliminary tests it was noted that the vertical jets tended to lean considerably in the same direction as flow in the diffuser section of the outfall. This leaning was caused by relatively high velocities in the diffuser and was reduced by increasing the outfall diameter. The final prototype outfall diameters of 20, 20, and 30 in. for the 3-, 6-, and 9-in. ports, respectively, minimized plume lean to the point that the height of the jets was not significantly affected, though the plume center line still deviated to the positive side (left side looking downstream) of the flume axis. While it was desirable to minimize plume lean in the model so that the analysis would be more straightforward, this lean could be an asset in a prototype situation where the longer plume arc length could increase overall mixing.

Brine solutions were prepared identically for both jet geometry and dilution tests. Sufficient fine-grain salt was dissolved in about 120 ft^3 of fresh water to attain the desired density differential between the brine effluent and the ambient fresh water. A red food coloring was then added in sufficient quantities to give even the diluted brine a discernible color contrast with the ambient flow. After repeated density checks with hydrometers indicated that the salt had dissolved completely, the brine was pumped through the appropriate Rotameter or venturi and into the outfall and diffuser. When visual observations indicated that a steady-state condition had been reached, tests were initiated. Ambient and brine flow rates were checked frequently during tests to maintain steady-state conditions.

B. Jet Geometry Tests

Either one or two movie cameras were used to photograph the brine plume in the vertical plane through the periscope. The cameras were aimed at points 17 ft (prototype) above the flume floor, and at points 20 and 100 ft downstream. After a steady-state condition had been established in the flume, the camera(s) were turned on for approximately 10 sec. A visual sketch of the plan view spreading of the brine was then made from above the flume for about half the tests. Flow conditions were changed, and the entire procedure was repeated. Table 1 shows the test conditions for which jet geometry data were taken (see Appendix A for Notation).

C. Dilution Tests

Tests for downstream dilution were run separately from those for jet geometry, although tests having identical flow conditions were given the same number. Each series of dilution tests was preceded by a recalibration of the conductivity probes. The probes were physically prepared by filing the copper electrodes lightly to remove any surface corrosion, the buildup of which results in output signal oscillation and drift. The adjustable bridge potentiometer was set to a value that would accommodate the expected range of conductivity. Several (three or more) calibration solutions were prepared, the first of which was pure ambient fresh water and the others were fresh water with enough brine solution added to give a range of conductivity readings up to full scale. Each probe to be used was dipped into each solution, and the temperature and conductivity were recorded. Later, the solution densities were determined on a specific gravity balance, and the corresponding temperature was again recorded. The procedure for reducing these calibrations is discussed in Appendix B.

The objective of the far-field dilution testing was to quantify the three-dimensional mixing patterns for a given operating condition from the peak of the dense plume to the downstream point where the brine spread laterally to the walls of the flume. Accordingly, conductivity-temperature probes were positioned at a number of downstream stations and detailed vertical profiles of conductivity and temperature were taken at each location with one probe at a time. Each conductivity-temperature measurement consisted of the following steps: (1) chart recorder turned on, stopwatch and integrating circuit simultaneously started; (2) temperature recorded; (3) stopwatch and integrating circuit simultaneously stopped; (4) chart recorder turned off; (5) integrating circuit voltage divided by run time and multiplied by calibration factor to get time-averaged conductivity; (6) maximum and minimum conductivity read from recorder; (7) all instruments zeroed for the next test. The ambient freshwater conductivity was also recorded for each probe as it was being used.

The basic dilution testing was conducted using a 6-in. prototype port with a density difference of about 0.021 g/cc. A few spot checks were made using an 0.01 g/cc differential, and several tests were conducted with 3- and 9-in. ports at 0.021 g/cc. A multiple-port, 20-in.-diam outfall and diffuser, with four 6-in. ports spaced at 13 ft, was tested with a density differential of 0.021 g/cc, and a 20-in.-diam simple outfall discharging horizontally with flow rates equivalent to that of the four-port diffuser was tested for comparison.

A limited test using heated brine was conducted to determine whether or not the temperature differential itself was an important factor influencing mixing. Two large space heaters were placed next to a 55-gal drum in which a brine solution was prepared. A temperature probe was installed inside a 20-in.-diam diffuser at the 6-in. port. The brine density in the heated drum was adjusted to maintain approximately an 0.021 g/cc density differential at the port. Limited downstream conductivity-temperature measurements were made, the brine temperature ranging from 4.5 to 9.4°C above the ambient temperature during the brief test.

Flow rates were checked frequently, and a visual sketch of the lateral brine spread was made for each test. Table 2 shows the dilution tests conducted. Fig. 5 presents typical plume characteristics as determined in a given test.

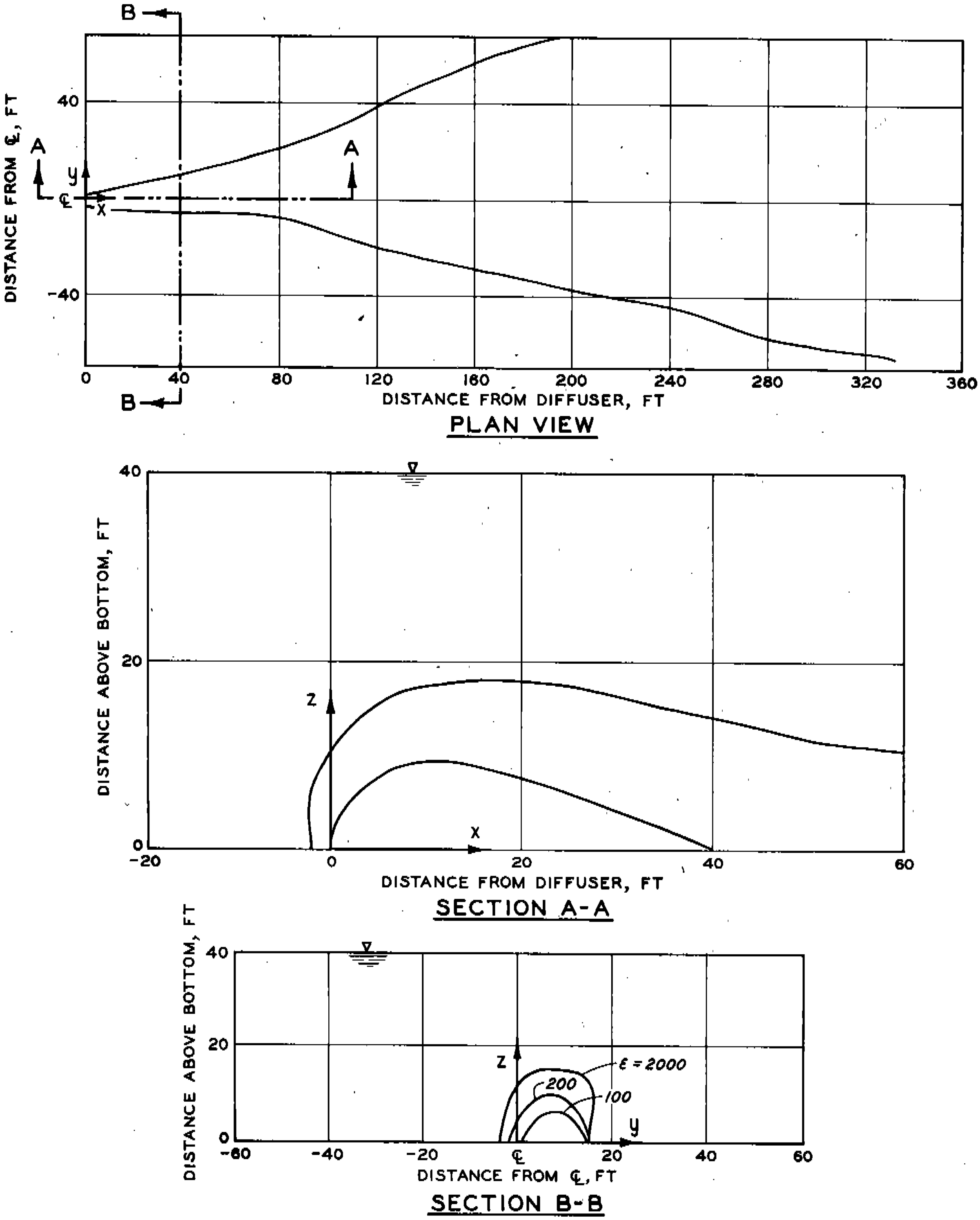

Fig. 5. Typical plume characteristics (test 639)

SECTION V: DATA REDUCTION AND ANALYSIS

A. Maximum Height of Jet

The movie of a grid of known dimensions photographed at the flume center line was projected onto graph paper and the distance of the projector from the paper adjusted so that the scale of jet tracings would be 1 in. to 10 ft prototype. The scale is exact only at the center of the frame; distortion increases toward the edges of the film. Movies of colored brine plumes were projected onto graph paper, and the projector was stopped periodically so that average tracings of the shape of a plume could be made as far downstream as the color contrast permitted. A typical profile is shown in fig. 5. Appendix C (under separate cover) contains the original tracings acquired in this manner, to a scale of one major division = 10 ft prototype. Due to distortion, the apparent plume origin does not coincide with the grid origin exactly.

From each plume tracing, Z_m , the maximum height of the upper boundary of the jet, was noted and recorded (see table 1). In cases where no distinct peak was evident, the height of the upper boundary directly above the point where the lower plume boundary peaked was taken as Z_m .

During testing, it was noted that for equivalent flow conditions, the maximum height of the plume increased as the port diameter was increased. This is explained as follows. Upon its discharge from a port, the plume consists essentially of a uniform, undiluted core of constant velocity that is eroded by turbulent mixing with the ambient fluid until the turbulence has progressed all the way to the center of the plume. The undisturbed central core is being decelerated only by a modified gravity force, while the outer turbulent regions are primarily being slowed by momentum exchange with the ambient fluid. Thus, the maximum height of a plume is related to the distance required for the turbulent erosion to spread into the central core, this distance being greater for a thick jet than for a thin one.

Keffer and Baines[2] found in studies of a turbulent neutrally buoyant air jet perpendicular to an ambient stream that a significant parameter was the ratio of the initial jet velocity to the free stream velocity. For a dense jet it is reasonable to expect that the density difference between the jet and the ambient fluid will affect the trajectory to some degree before the plume reaches a peak, and significantly thereafter. Studies conducted by Dow Chemical Company[1] determined that for dense jets discharging at various angles into a still fluid the normalized maximum jet height is a linear function of densimetric port Froude number. Therefore, in attempting to develop an equation for the prediction of the maximum jet height, it was assumed that

$$\frac{Z_m}{D_o} = f\left(\frac{V_o}{U}, \mathbb{F}_D , \frac{\Delta\rho_m}{\rho_f}\right) \tag{1}$$

where

Z_m = maximum height of upper boundary of the plume

D_o = port diameter

U = free stream velocity

V_o = initial port discharge velocity

$\mathbb{F}_D$ = densimetric port Froude number, $\dfrac{V_o}{\sqrt{\dfrac{\Delta\rho_m}{\rho_f} gD_o}}$

$\Delta\rho_m$ = initial density differential between brine and ambient fluid

ρ_f = density of ambient fluid

Correlations of (1) Z_m/D_o versus $\mathbb{F}_D$ for constant V_o/U, (2) Z_m/D_o versus V_o/U for constant $\mathbb{F}_D$, and (3) Z_m/D_o versus V_o/U for constant $\Delta\rho_m/\rho_f$ all yielded equations for Z_m/D_o that satisfied most of the data but appeared to be invalid at the lower ambient velocities. This indicated that the separate effects of the dimensionless variables were being neither fully isolated nor accounted for over the entire range of flow conditions. This conclusion was confirmed by visual observations of erosion and dispersion of the jets. The dispersion in the near field appeared to be predominantly influenced by the turbulence of the jet itself or densimetric Froude number (though admittedly the pressure field and turbulence of the flowing fluid are pertinent to near-field jet dispersion), while the far-field dispersion can be primarily attributed to the relative intensity of turbulence in the far-field plume, or density current, and that of the ambient channel flow. This relative turbulence is considered to be related to the ratio of ambient to port velocities, U/V_o. Therefore, it was decided that analysis of data would be made in a manner such that correlation of the interrelations of U/V_o and $\mathbb{F}_D$ would be included in an empirical coefficient much as the frictional and form drag components are represented by an empirically determined drag coefficient.

At a conference on the study, Professor R. O. Reid of Texas A&M University indicated that Fan[3] had found the product $(U/V_o)\mathbb{F}_D$ to be a significant parameter. Least-squares correlations of Z_m/D_o versus $\mathbb{F}_D$ were made at WES for constant values of $(U/V_o)\mathbb{F}_D$, resulting in equations of the form

$$\frac{Z_m}{D_o} = C\mathbb{F}_D + B \qquad (2)$$

where B is a random intercept whose mean value is essentially zero and

$$C = \phi\left(\frac{U}{V_o}\,\mathbb{F}_D\right) \tag{3}$$

A plot of the predicted versus observed Z_m/D_o values indicated that the prediction equation was valid over the entire range of variables. The scatter was improved somewhat by accounting for the outfall diameter, D, which as reproduced in the model had the effect of elevating the entire jet a small amount. Thus Z_m/D_o was replaced by $(Z_m - D)/D_o$, and least-squares correlations of $(Z_m - D)/D_o$ versus $\mathbb{F}_D$ for constant $(U/V_o)\mathbb{F}_D$ were repeated, leading to the following equation:

$$\frac{Z_m - D}{D_o} = C\mathbb{F}_D \tag{4}$$

$$C = 3.4 \times 10^{-0.148(U/V_o)\mathbb{F}_D} \tag{5}$$

$$Z_m \leq H \tag{6}$$

Fig. 6 is a plot of actual versus predicted values of $(Z_m - D)/D_o$.

B. Lateral Spread of Jet

Superposition of single-port dilution results to predict multiple-port characteristics requires prediction of the lateral spread of the plume. As discussed in the previous section, visual sketches of the lateral spread of the dense effluent were made for approximately half of the jet geometry tests. From these sketches, w, the observed horizontal width of the plume irrespective of the plume center line, was measured and recorded along with x, the corresponding downstream distance from the diffuser. These selected sets of coordinates, the number of which is determined by the downstream length required for the brine to spread to the edges of the flume floor for each test, are given in table 3.

The lateral spread can generally be divided into two regions: (1) before the arcing plume has settled to the bottom, and (2) after this point, when spread is generally more rapid. For a single test, w correlates linearly with x for each region as defined above. The slopes and intercepts of these correlations were related to the ambient velocity, port velocity, etc.

In attempting to develop a method for prediction of the lateral spread, three general approaches were considered and are briefly described as follows:

(1) Compute the least-squares slopes and intercepts of individual

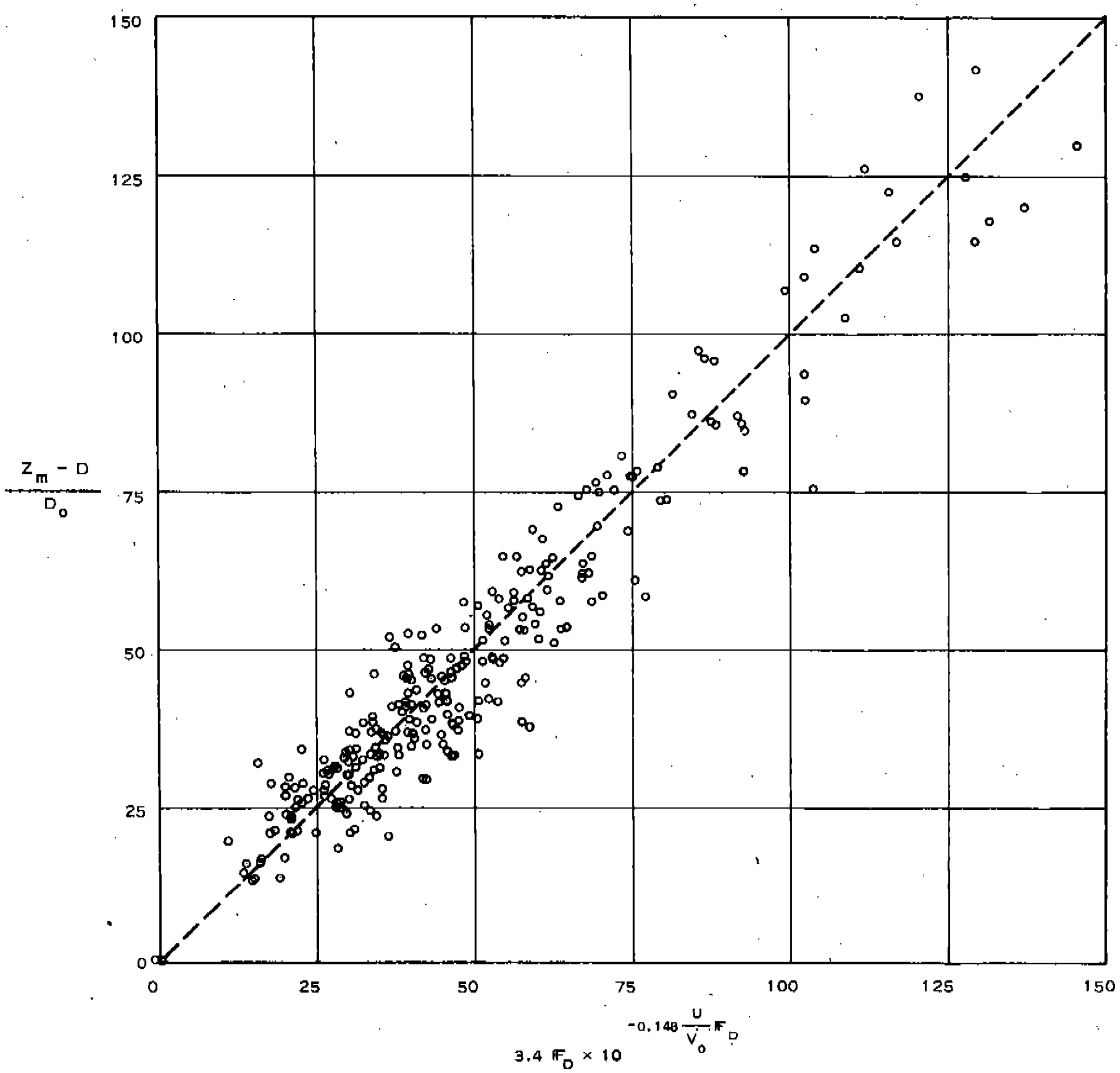

Fig. 6. Actual versus predicted values of dimensionless jet height according to equation 4

linear correlations of w/D_o versus x/D_o for each region. Determine their functional dependence on the relevant flow parameters.

(2) Normalize w and x by $D_o(V_o^2/U^2)$ as suggested by Keffer and Baines.[2] Relate $wU^2/D_oV_o^2$ to $xU^2/D_oV_o^2$ in terms of relevant flow parameters.

(3) Defining x_o and w_o as the downstream distance at which the plume falls to the bottom and its width at that point, respectively, determine x_o and w_o as functions of $\mathbb{F}_D$, Z_m/D_o , and $(U/V_o)\mathbb{F}_D$. Then correlate x/x_o with w/w_o in terms of other flow parameters for both regions.

Approach 1 above yielded fair estimates of the lateral spread, but with enough systematic deviations from a perfect prediction to warrant a different approach. The success with which a modified Froude number, $(U/V_o)\mathbb{F}_D$, was used to predict the maximum jet height indicated that approach 3 was worthy of consideration.

Use of this approach first requires a means of predicting x_o and w_o . For roughly 100 of the lateral spread sketches, x_o could be approximated by the downstream distance at which the initial linear rate of spread changed to a more rapid rate. This point was often difficult to define, especially for the higher ambient velocities; all values thus determined were checked against the corresponding plume trajectory sketches (Appendix C) and a few unreasonable values revised. Values of w_o , the total width of the plume at x_o , were concurrently recorded.

Following the general approach of the maximum jet height correlations, x_o/D_o was correlated with $\mathbb{F}_D$ for constant values of $(U/V_o)\mathbb{F}_D$. Individual log-log correlations were reasonably good, but their slopes and intercepts could not be correlated consistently with $(U/V_o)\mathbb{F}_D$. A more successful correlation resulted from linear plots of x_o/D_o and Z_m/D_o for constant $(U/V_o)\mathbb{F}_D$, where Z_m/D_o has been assumed nearly equal to $(Z_m - D)/D_o$. Forcing these correlations to pass through the origin (assuming $x_o = 0$ when $Z_m = 0$), their slopes were found to be a logarithmic function of $(U/V_o)\mathbb{F}_D$. An identical procedure was used for w_o/D_o , and the following empirical equations resulted:

$$\frac{x_o}{D_o} = 9.62 \log_{10}\left(2 \frac{U}{V_o} \mathbb{F}_D\right)\frac{Z_m}{D_o} \tag{7}$$

$$\frac{w_o}{D_o} = 1.51 \log_{10}\left(4.91 \frac{U}{V_o} \mathbb{F}_D\right)\frac{Z_m}{D_o} \tag{8}$$

Having developed a means of predicting x_o and w_o , the relation between x/x_o and w/w_o could now be investigated. The coordinates of total spread, as included in table 3, were divided by predicted values of x_o and w_o for each of the 187 tests for which sketches were made, and x/x_o was plotted against w/w_o for constant values of $(U/V_o)\mathbb{F}_D$. Least-squares linear fits of these log-log correlations (which by definition passed through $x/x_o = 1.0$, $w/w_o = 1.0$) clearly indicated an increase in rates of spread when $x/x_o > 1$, as was suggested by qualitative observations. The rates of spread were found to be an exponential function of $(U/V_o)\mathbb{F}_D$ for $x \le x_o$, and a logarithmic function for $x > x_o$. Thus

$$\frac{w}{w_o} = \left(\frac{x}{x_o}\right)^R \tag{9}$$

where

$$R = 3.02 \times 10^{-0.26(U/V_o)\mathbb{F}_D} \quad \text{for} \quad x \le x_o \tag{10}$$

and

$$R = 0.61 \log_{10}\left(4 \frac{U}{V_o} \mathbb{F}_D\right) \quad \text{for} \quad x > x_o \tag{11}$$

Fig. 7 is a plot of observed values of w/w_o versus the values predicted using equations 7-11. Although there is a broad band of scatter due to errors in visually sketching the lateral spread and subjectively determining x_o and w_o, the overall trend indicates a valid prediction over the entire spread regime.

C. Dilution for Single-Port Tests

A convenient dimensionless representation of mixing is dilution, defined as

$$\epsilon = \Delta\rho_m / \Delta\rho$$

where

$\Delta\rho_m = \rho_b - \rho_f$

$\Delta\rho = \rho - \rho_f$

ρ_b = initial brine density, g/cc

ρ_f = ambient density, g/cc

ρ = density at some point in the far-field mixing region, g/cc

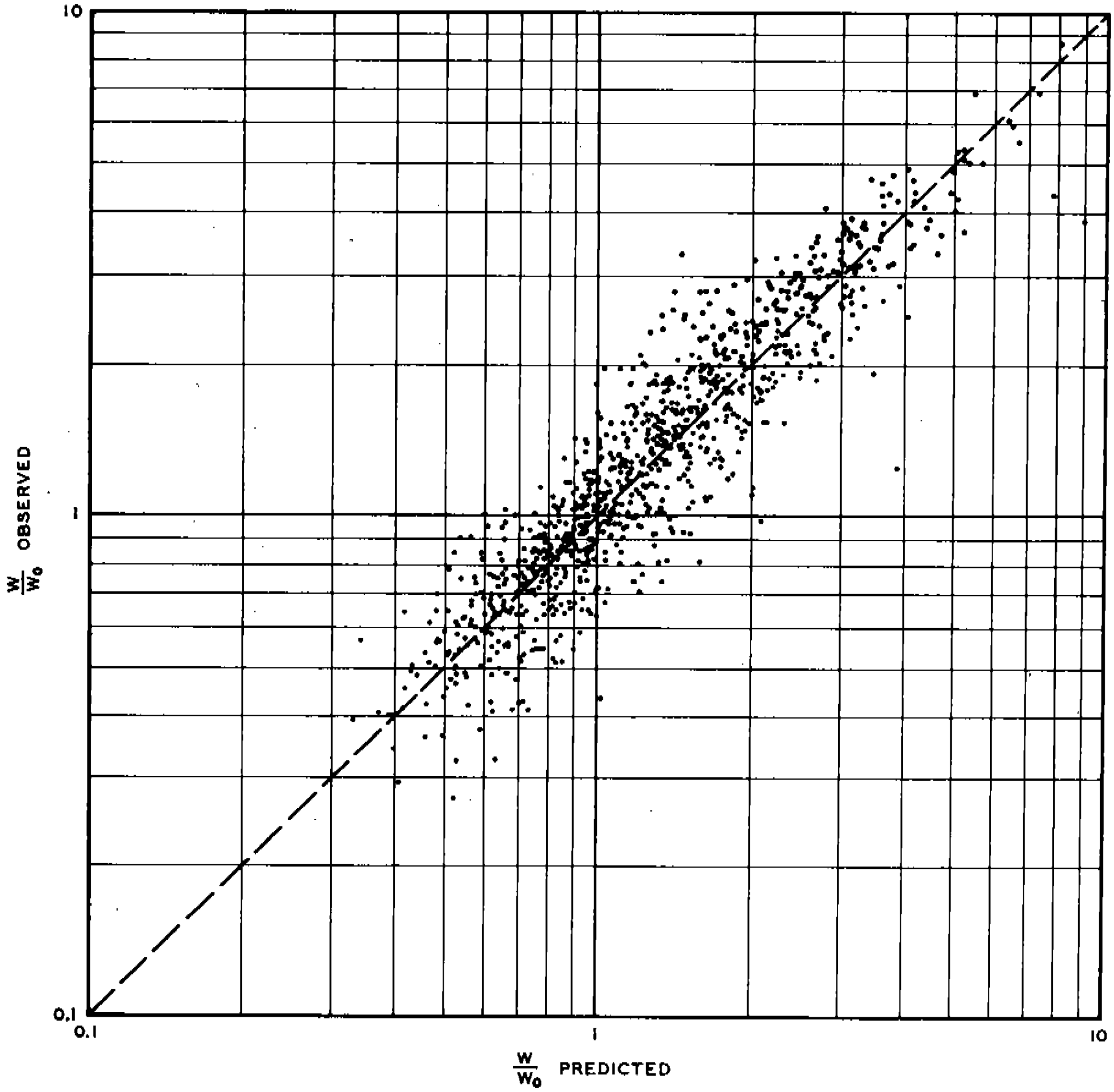

Fig. 7. Observed values of dimensionless plume width versus values predicted by equations 7-11

As defined above, the dilution of pure unmixed brine is 1.0 and that of undisturbed ambient fluid is infinity. The FORTRAN program described in Appendix B was used to calibrate the conductivity probes and to compute dilution values corresponding to minimum, average, and maximum conductivity readings at a point. Table 2 is a list of dilution test conditions. Average dilution values have been plotted at each longitudinal station for each test, and contours of constant dilution have been sketched. The resulting plots to a scale of one major division = 20 ft prototype are presented under separate cover in Appendix D. Fig. 5 is a typical sketch of dilution contours at a given cross section. The outer edges of the diluted plumes are difficult to define with precision, as the conductivity probe calibrations for salinities near the ambient salinity are extremely sensitive to slight shifts in the background conductivity. In attempting to define the limits, it should be noted that dilutions of 100, 500, and 2000 represent a 99.00, 99.80, and 99.95 percent reduction of the initial density differential, respectively.

The scope of this project prohibited any attempts to generalize the complete downstream mixing patterns. However, it was feasible to develop a prediction of the minimum dilution (i.e. maximum concentration) to be expected at any longitudinal distance from the diffuser. In general, the dilution increases with ambient velocity and downstream distance and decreases with increasing port diameter and discharge velocity.

Again, referring to the Keffer and Baines[2] dimensionless downstream length defined as

$$\frac{xU^2}{D_o V_o^2}$$

and defining the minimum dilution as ϵ_m , one might expect that

$$\epsilon_m = f\left(\frac{xU^2}{D_o V_o^2}\right) \tag{12}$$

From the dilution data for each test, the minimum observed dilution ϵ_m , which generally was at the center of a free plume and at the bottom of brine flow along the floor, was tabulated for each longitudinal position x . These values were then plotted against $xU^2/D_oV_o^2$ on log-log axes. A general correlation was indicated, but with systematic scatter suggesting that the maximum jet height Z_m had additional bearing on the overall mixing. A second correlation using $\epsilon_m/(Z_m/D_o)$ in place of ϵ_m diminished the systematic scatter, and a final log-log plot of

$$\frac{\epsilon_m}{(Z_m/D_o)^2} \text{ versus } \frac{xU^2}{D_o V_o^2} \tag{13}$$

displayed good overall correlation with random scatter (fig. 8). The data for ambient velocity of 0.1 knot tended to correlate separately from the data for all other ambient velocities. The scatter in fig. 8 is due to small errors in the calibration and data reduction procedure as well as to the likelihood of "missing" a true minimum dilution which fell between discrete vertical or horizontal sampling points.

The above correlation was made before the potential of using $(U/V_o)\mathbb{F}_D$ to predict jet geometry characteristics had been fully realized. Thus a new attempt to correlate the data was made along the lines of the maximum jet height and lateral spread approaches. Dilution is a measure of the degree to which ambient fluid is entrained into the brine plume. This entrainment is also the mechanism by which the plume spreads, increasing its total cross-sectional area and effective discharge. Thus the dilution should be a direct function of the rate of increase of plume area, as well as w, a parameter characteristic of the cross-sectional area. Since w/w_o correlated directly with x/x_o for constant values of $(U/V_o)\mathbb{F}_D$, an obvious approach is to correlate the minimum dilution, ϵ_m, with x/x_o for constant values of $(U/V_o)\mathbb{F}_D$.

Correlations made in this manner indicated that the log-log slopes were not a function of $(U/V_o)\mathbb{F}_D$, but appeared to be a single constant value for $x/x_o \le 1.0$ and $x/x_o > 1.0$. The log-log intercepts vary exponentially with $(U/V_o)\mathbb{F}_D$, and the resulting equation is as follows:

$$\epsilon_m = \left[31.0 \times 10^{0.4(U/V_o)\mathbb{F}_D}\right] \left(\frac{x}{x_o}\right)^{0.68} \tag{14}$$

Fig. 9 is a plot of observed values of ϵ_m versus the corresponding predictions using equation 14. The prediction is quite good considering the difficulties in obtaining good dilution data and probe calibrations, and appears to be valid for the entire range of ambient velocity.

D. Multiple-Port Dilution Comparison

The data reduction procedures described above for the single-port dilution tests were applied to the five multiple-port diffuser tests. The resulting dilution contour plots are presented under separate cover in Appendix D.

The primary purpose of the multiple-port tests was to determine whether or not superposition of single-port results is a valid technique for prediction of multiple-port mixing. Accordingly, the single-port results of tests 655, 659, 671, and 675 were conceptually overlaid to simulate four identical plumes spaced at 13 ft o.c.; the dilution values at a single downstream station were calculated assuming linear superposition of the separate overlapping dilution contours. Fig. 10 is a plot of the calculated and observed contours; note that for tests 671 and 675 the comparison could not be made at identical downstream stations.

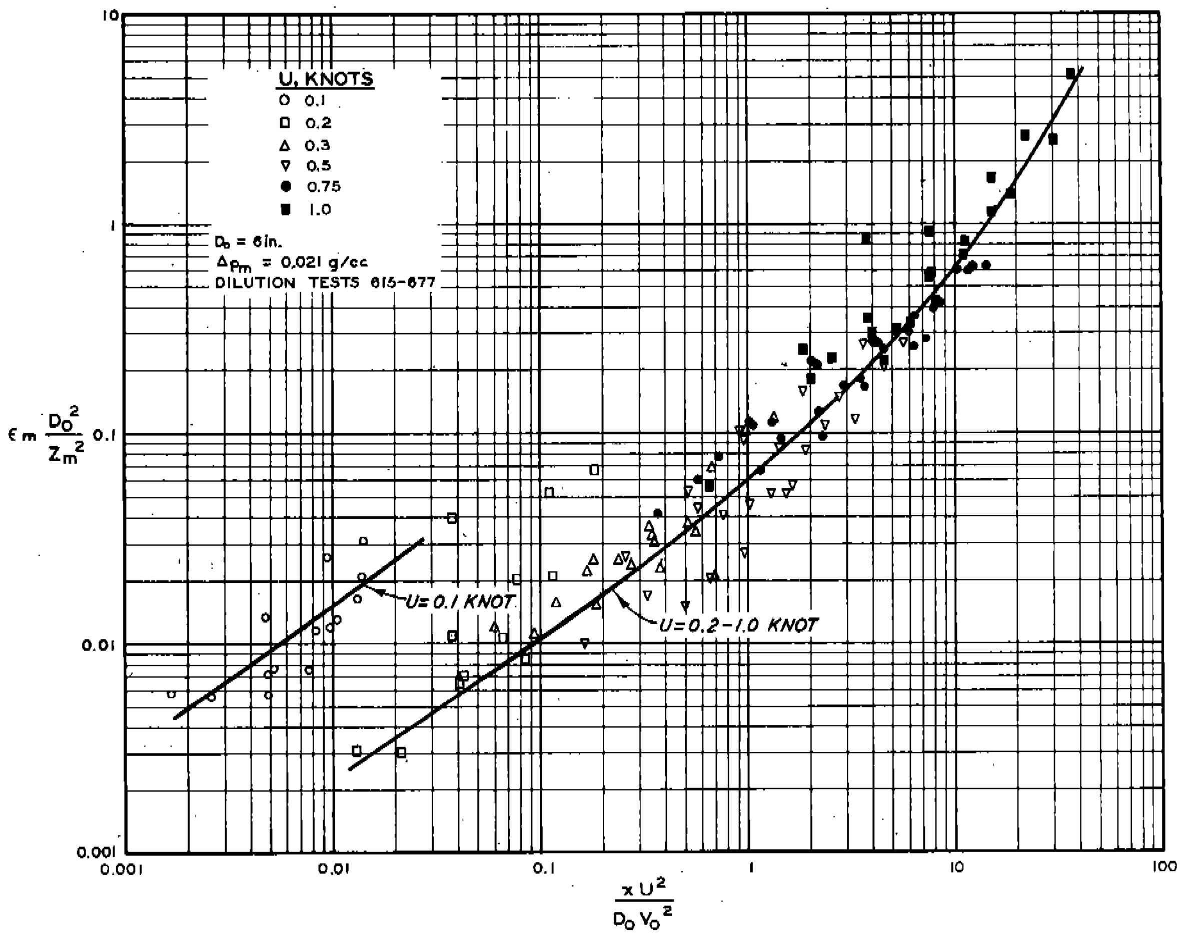

Fig. 8. Correlation of minimum dilution with dimensionless downstream distance

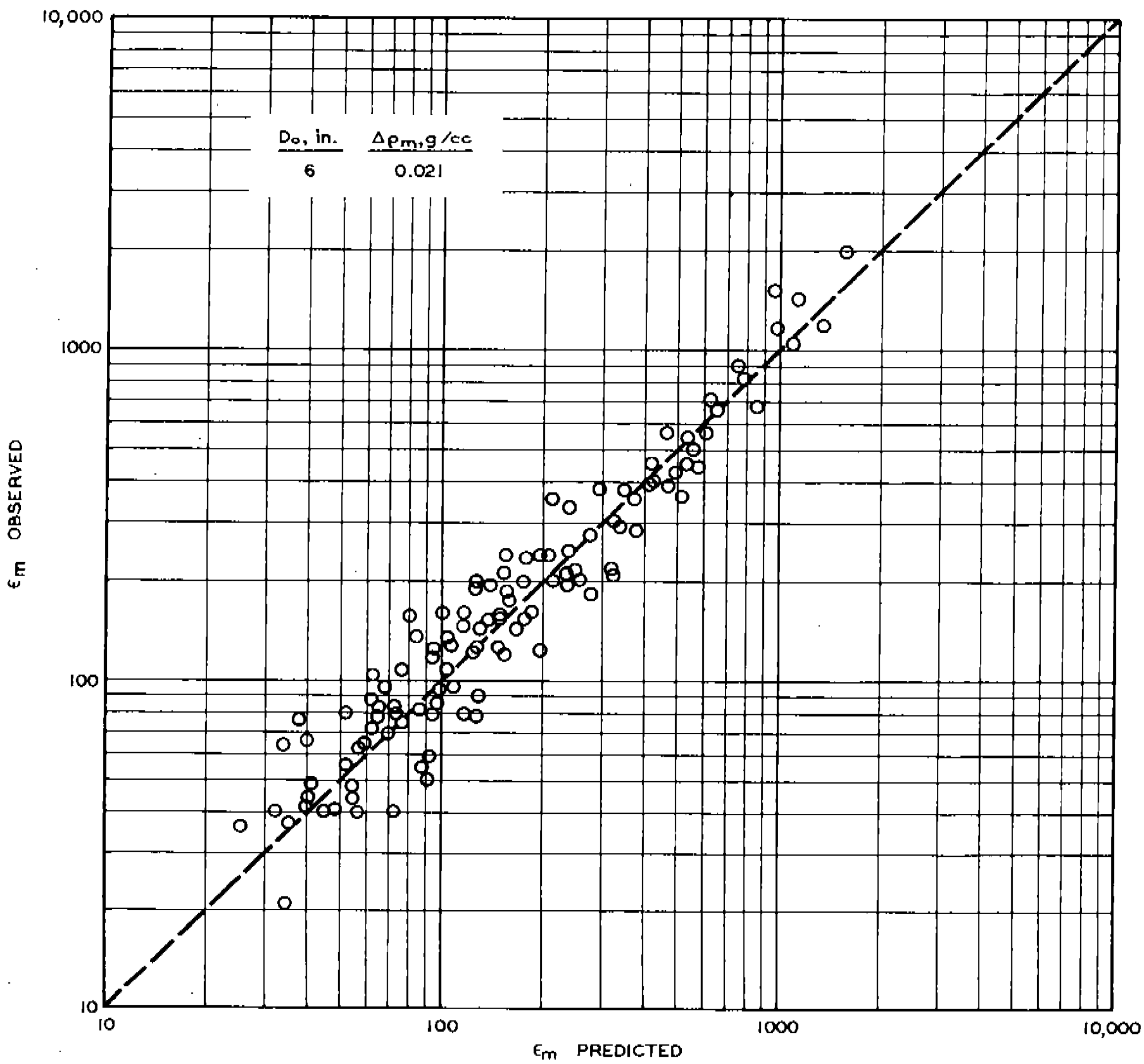

Fig. 9. Observed values of minimum dilution versus values predicted by equation 14

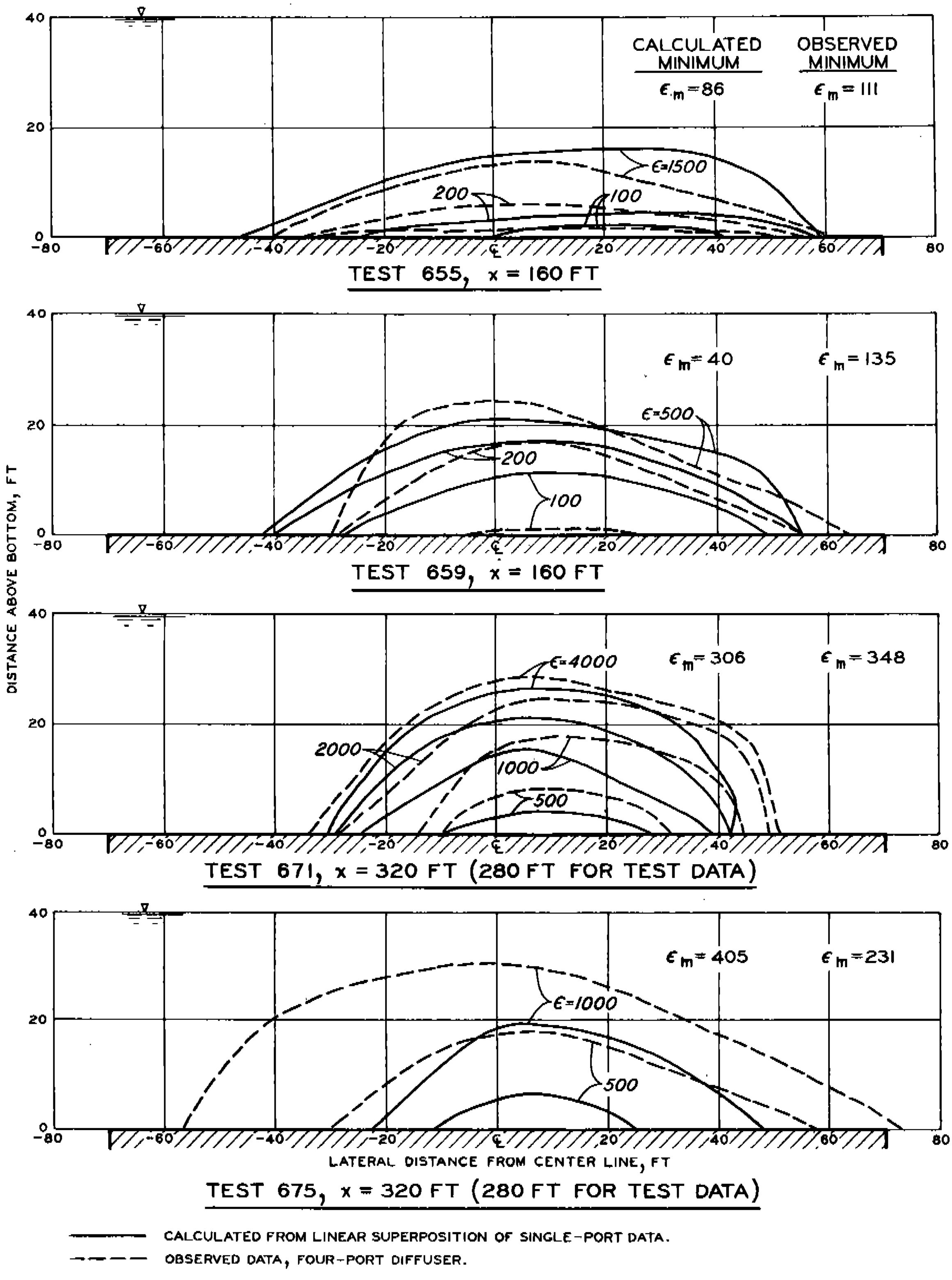

Fig. 10. Comparison of observed multiple-port dilution contours with superposition prediction (looking upstream)

The individual effects of the four separate plumes were essentially indiscernible downstream of the point where the jets merged. There appeared to be no hydrodynamic interaction between the plumes that might invalidate an assumption of linear superposition. Tests 4-655 and 4-659 agree quite well with the calculated predictions in terms of overall area of influence and degree of dilution. Tests 4-671 and 4-675 have been compared at $x = 320$ ft with superposition of corresponding plumes at $x = 280$ ft ; agreement is good for 4-671 but poorer for 4-675, possibly due to the sensitivity of the results to the probe calibrations. The superposition technique does appear adequate for prediction of downstream mixing patterns.

No attempt has been made as part of this study to generalize the dilution contours. If the contours could be approximated by Gaussian distributions (as was assumed by Crew [4]), the minimum dilution correlation could be used to construct a series of downstream concentration profiles that could then be superimposed to predict the mixing downstream of any multiple-port diffuser, assuming a level ocean floor.

E. Simple Outfall Comparison

The brine discharged horizontally from a 20-in.-diam simple outfall tended to remain in close proximity to the bottom. Therefore, it appeared most appropriate to compare the resulting dilution patterns with the corresponding multiple-port mixing on a two-dimensional basis. Figs. 11, 12, and 13 present the plan view contours of constant dilution for corresponding simple outfall and multiple-port diffuser tests.

While the above figures may not at first suggest a dramatic difference between the two schemes, it is important to recognize that the simple outfall places the highest concentrations directly onto the ocean floor; whereas, in terms of maximum concentrations, the effective point of discharge with the diffuser is located some distance x_o downstream from the outfall where the brine has undergone an initial dilution of the order of magnitude of 100 before impinging upon the bottom. Thus, a comparison of the two schemes on the basis of bottom area affected by a given concentration would demonstrate the clear advantage of the multiple-port diffuser in protecting the ocean floor environment.

The diffuser port diameters and flow rate used in these comparison tests resulted in port Froude numbers of about 13.1, a relatively low value. Had the Froude numbers been increased by reducing the port diameters, the distance x_o , and thus the initial dilution, would have been increased. An inherent advantage of the multiple-port diffuser is that the number and size of its ports can be adjusted to provide a range of initial dilutions.

F. Effect of Heated Brine

Fig. 14 is a comparison of the dilution contours for the heated brine test with those for test 657 for which all flow conditions except the temperature differential were equivalent. Agreement is quite good at $x = 40$ ft and 80 ft, and acceptable at $x = 120$ ft and 280 ft where low concentrations amplify the probe calibration error.

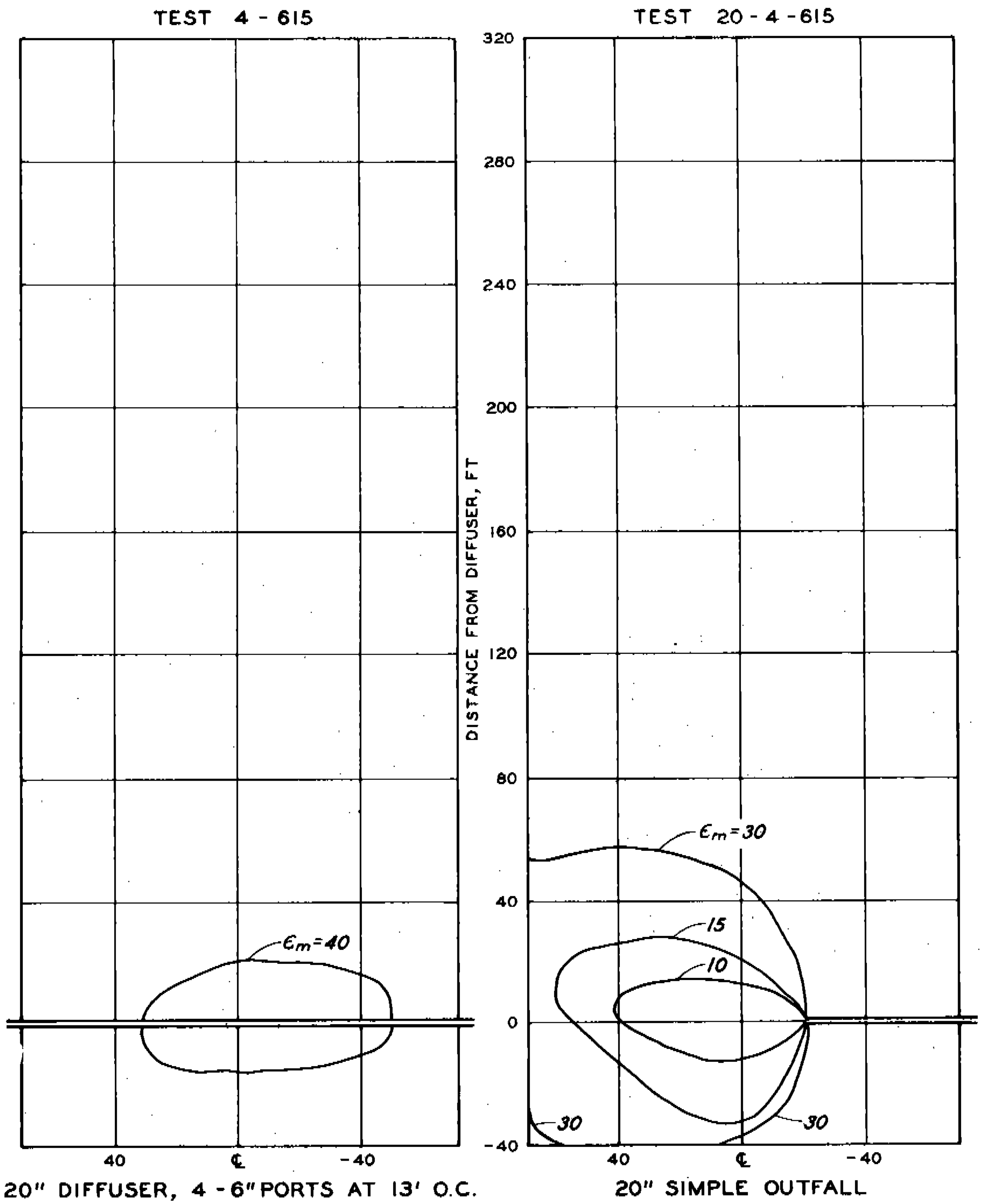

Fig. 11. Comparison of simple outfall and multiple-port diffuser; U = 0.1 knot, brine flow = 5.01 cfs, and $\Delta\rho_m$ = 0.021 g/cc. Contours of minimum observed average dilution

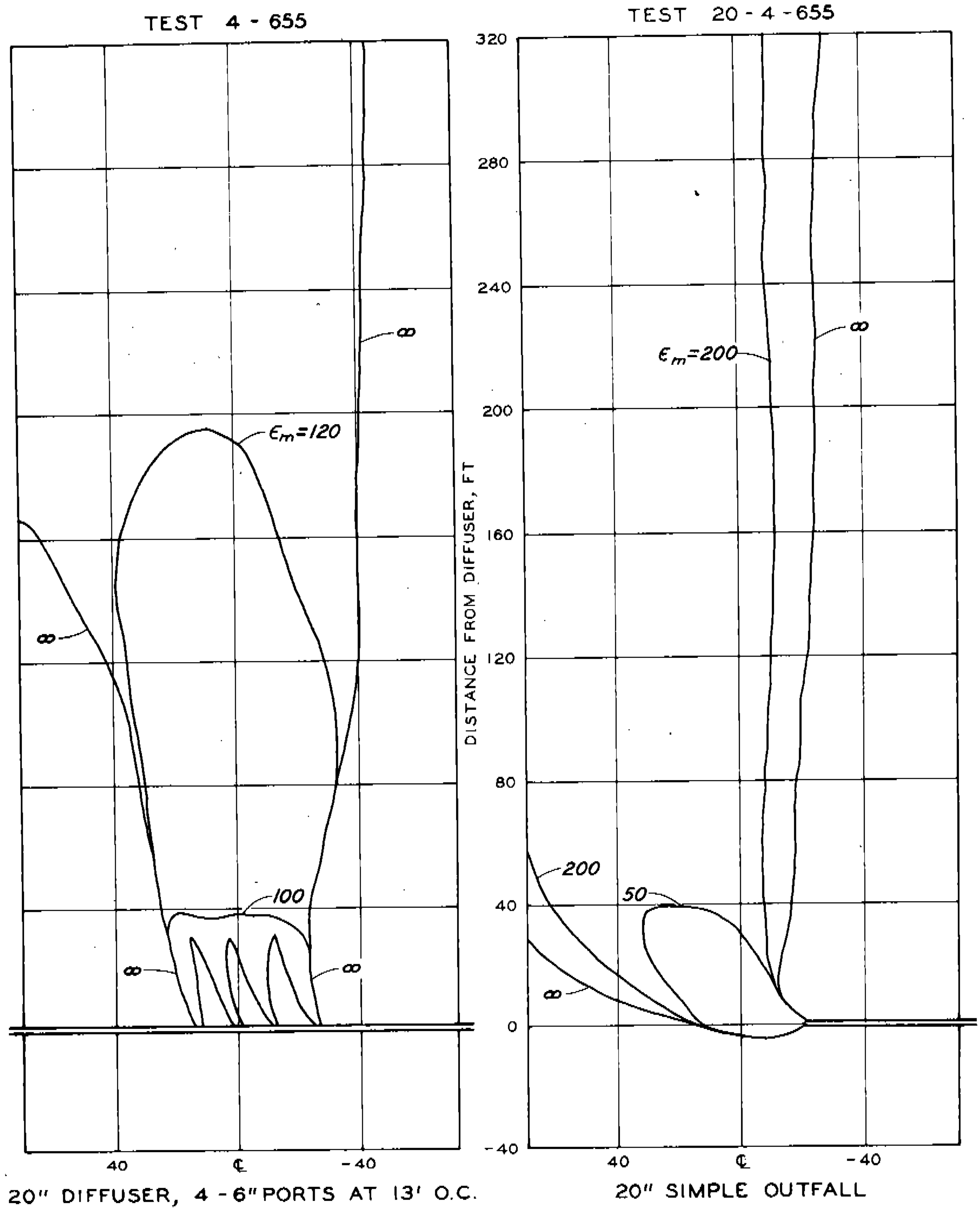

Fig. 12. Comparison of simple outfall and multiple-port diffuser; U = 0.5 knot, brine flow = 5.01 cfs, and $\Delta\rho_m$ = 0.021 g/cc. Contours of minimum observed average dilution

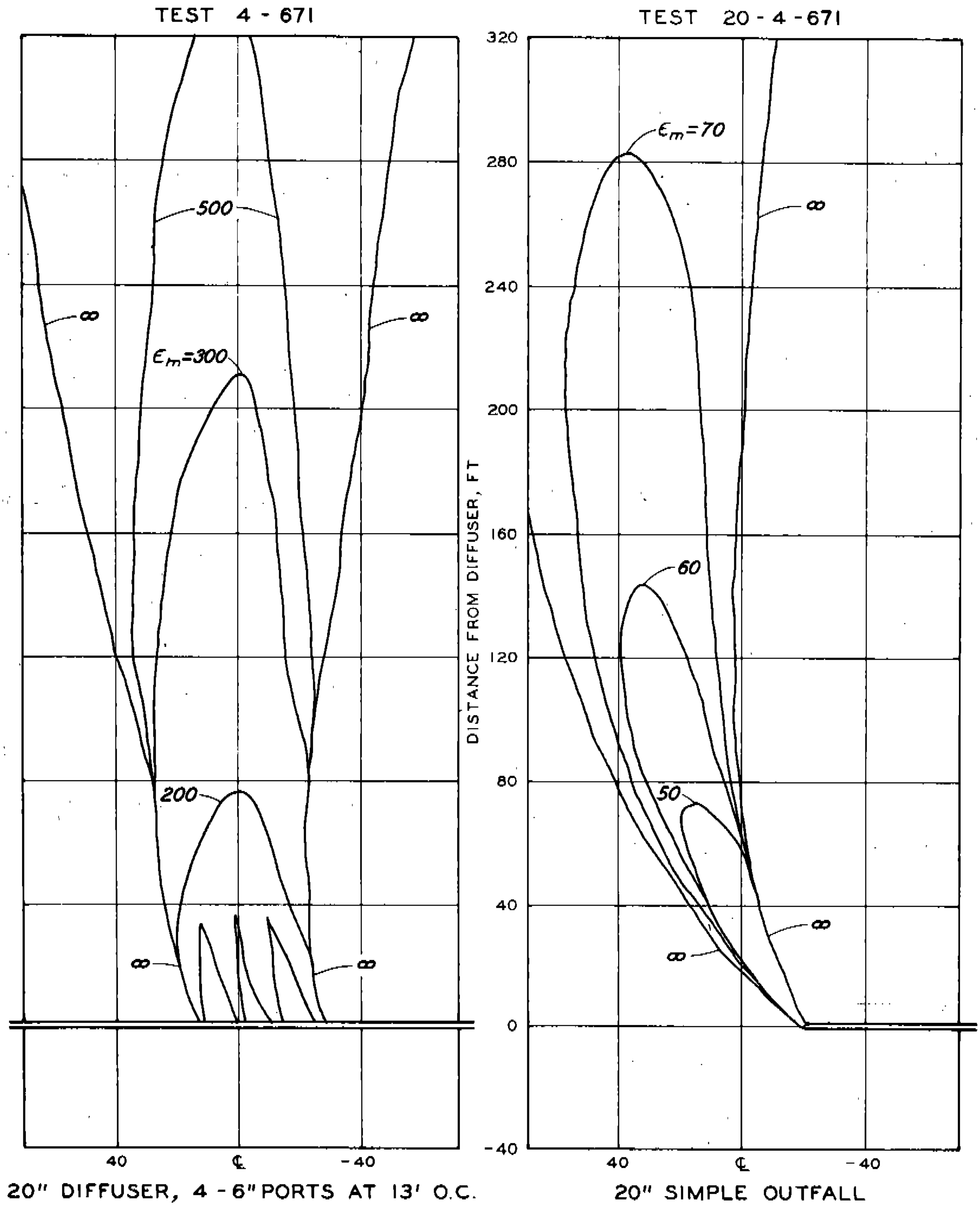

Fig. 13. Comparison of simple outfall and multiple-port diffuser; U = 1.0 knot, brine flow = 5.01 cfs, and $\Delta\rho_m$ = 0.021 g/cc. Contours of minimum observed average dilution

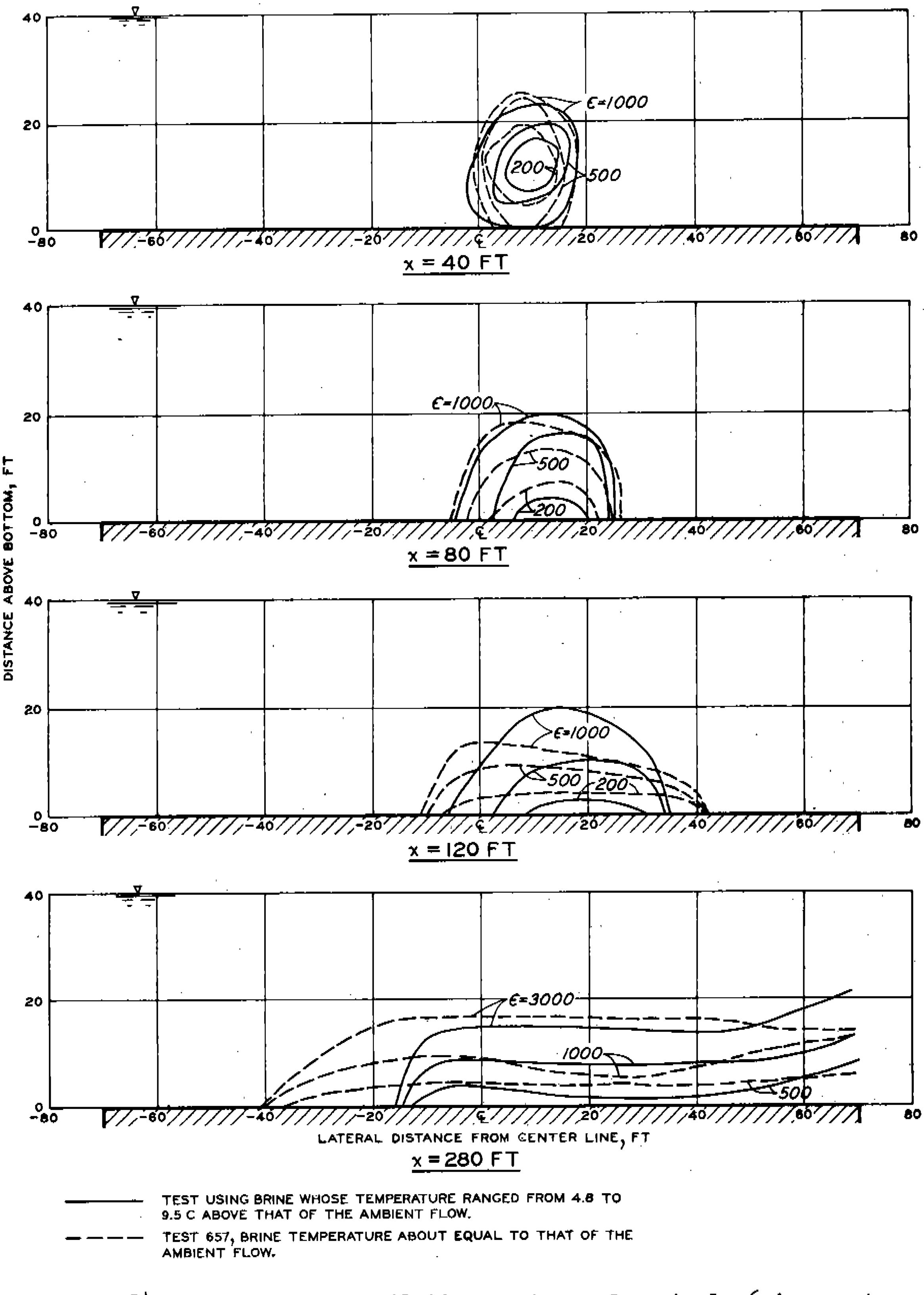

Fig. 14. Comparison of dilution contours for single 6-in. port for heated brine and test 657 (looking upstream); U = 0.5 knot, $\mathbb{F}_D$ = 18.7, $\Delta\rho_m$ = 0.021 g/cc

SECTION VI: DISCUSSION OF RESULTS

A. Maximum Height of Jet

Studies at WES of submerged jets associated with lock filling and emptying systems have indicated that ratios of outfall conduit area to port area (A_o/A_p) less than 1.05 result in greatly altered manifold and jet characteristics; for higher ratios, A_o/A_p is not considered to have an important effect on the distribution of flow in a multiple-port diffuser. In the present study, A_o/A_p ranged from 11.1 for the 6- and 9-in. ports to 44.5 for the 3-in. ports. The existence of only two values of A_o/A_p precluded any systematic evaluation of its effect on the jet characteristics. However, it was noted that separation of the data into two groups based on the area ratio indicated only a slight dependence on A_o/A_p, the scale of which was less than the experimental data scatter.

In a prototype situation, the level of turbulence in the ambient flow, and therefore the jet characteristics, could well be related to H, the total depth of flow. Although the few jet geometry tests run with $H = 30$ ft displayed no significant deviation, virtually all of the data taken here was for $H = 40$ ft, so that all empirical constants should be considered subject to possible dependence on the depth of flow.

Although testing was not conducted below an ambient velocity of 0.1 knot prototype, setting $U = 0$ in equation 4 yields

$$\frac{Z_m - D}{D_o} = 3.4\ \mathbb{F}_D \tag{15}$$

This compares quite well with the work of Turner[5] who predicted for a dense jet discharged vertically into a still fluid that

$$\frac{Z_m - D}{D_o} = 3.47\ \mathbb{F}_D \tag{16}$$

In considering the general shape of jets, it is obvious that the mushrooming, axisymmetrical vertical jet in still fluid undergoes a transition in becoming an arcing plume at small ambient velocities. A few tests were run in hopes of determining visually at what ambient velocity this transition takes place. Although the transition point is difficult to pinpoint objectively and is to some degree a function of the densimetric Froude number, an ambient velocity of $U = 0.07$ knot prototype can be thought of as the transition velocity.

B. Dilution Contours

Fig. 15 is an example of the extreme fluctuations in conductivity at a point due to the turbulent jet mixing. The level of fluctuations decreased

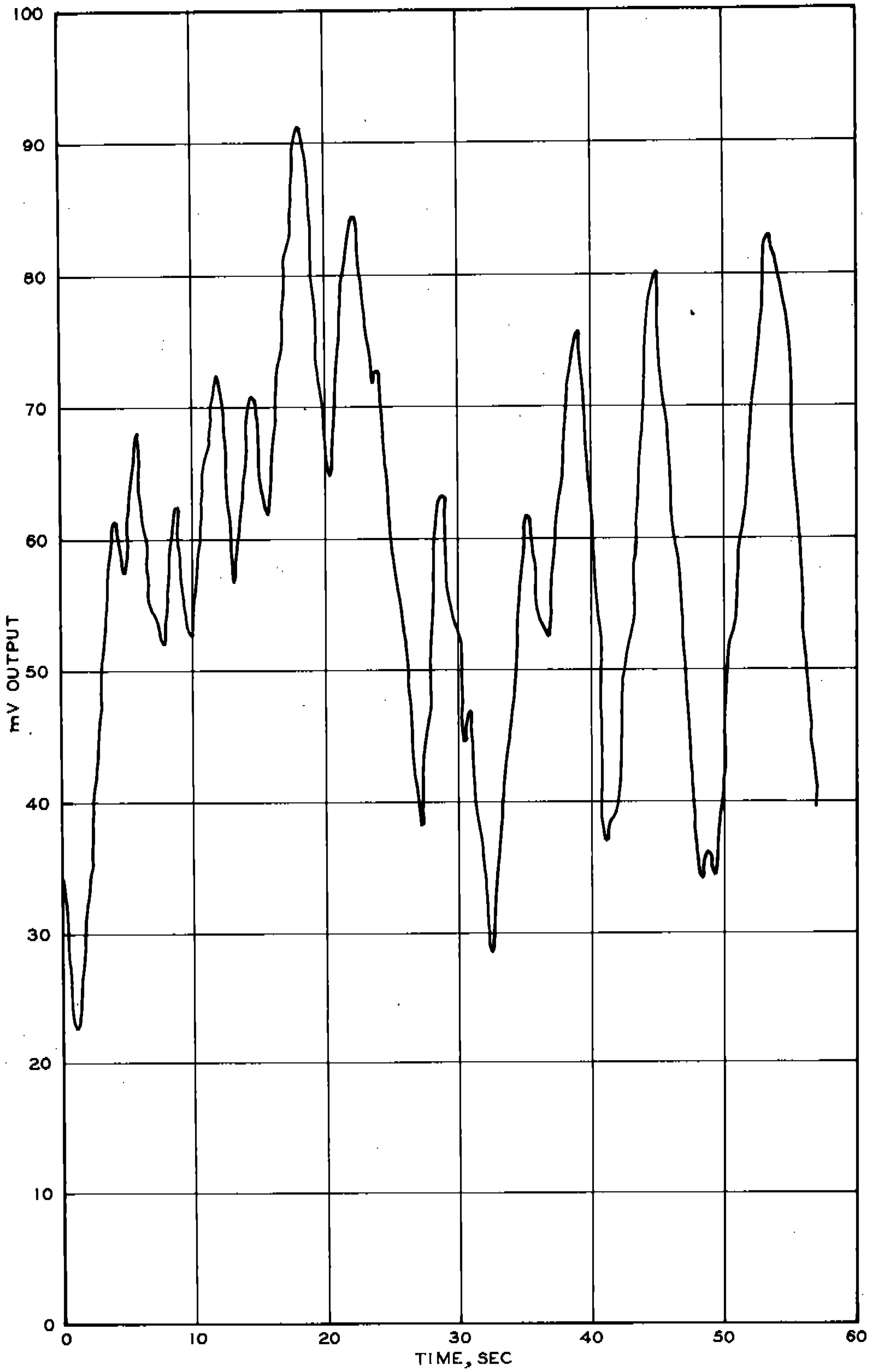

Fig. 15. Fluctuations in conductivity due to turbulent jet mixing

with distance downstream but remained significant enough that mean values could never be reliably estimated visually. As discussed earlier, 1-min samples of the conductivity probe output were processed by the integrating circuit to estimate mean values. A typical 24-min sample of conductivity output was analyzed statistically to verify the use of a 1-min sample time in actual testing.*

The overall mean of conductivities at 1-sec intervals was 61.7 mv, with a standard deviation of 10.5 mv; the total range of conductivity was from 26 to 91 mv. The sample distribution was reasonably close to a Gaussian curve with the same mean and standard deviation. Analysis of the mean values for the twenty-four 1-min samples gave a standard error of estimate of 4.5 percent. Doubling the sample time to 2 min would reduce this to 3.4 percent. The relatively small reduction in the standard error of estimate for a doubling of the sample time is considered to justify the use of a 1-min record in predicting mean values.

The dilution patterns cannot qualitatively be compared with the numerical contours predicted by Crew[4] without evaluating the vertical turbulence exchange coefficient, a quantity that scales the dimensionless parameters used in the numerical formulation. This coefficient is a function of the scale and intensity of turbulence and was not evaluated for the WES flume. However, qualitatively the experimental contours confirm the numerical predictions of an arcing plume falling to the bottom and spreading as a gravity wave toward the flume walls as it is swept downstream.

The numerical model assumed a plane horizontal flume bottom, as was the case in the WES flume. However, tests of model diffusers in distorted estuary models at WES, reported under separate cover as Part II of this report, indicated that bottom depressions tend to fill up with relatively high concentrations of dense effluent, controlling the spread of the brine to a significant extent. Therefore, it is important to recognize that bottom irregularities in the prototype situation may cause large localized deviations from the model predictions.

C. Correlation of Dilution with Dimensionless Downstream Distance

The dilution correlation presented in fig. 9 and discussed earlier was made with data using $D_o = 6$ in. and $\Delta\rho_m = 0.021$ g/cc. Six additional tests were run with varying values of $\Delta\rho_m$ and D_o and the minimum dilution values for these tests are plotted in fig. 16 for comparison with the previous dilution correlation.

Nearly all the predicted dilutions were less than the observed values. This indicates that the previously developed prediction equation, equation 14, is not valid in general, but strictly speaking can be applied only when $D_o = 6$ in. and $\Delta\rho_m = 0.021$ g/cc. However, the points plotted on fig. 16

* Personal communication; analysis conducted by Professor R. O. Reid, Texas A&M University, Department of Oceanography, College Station, Tex.

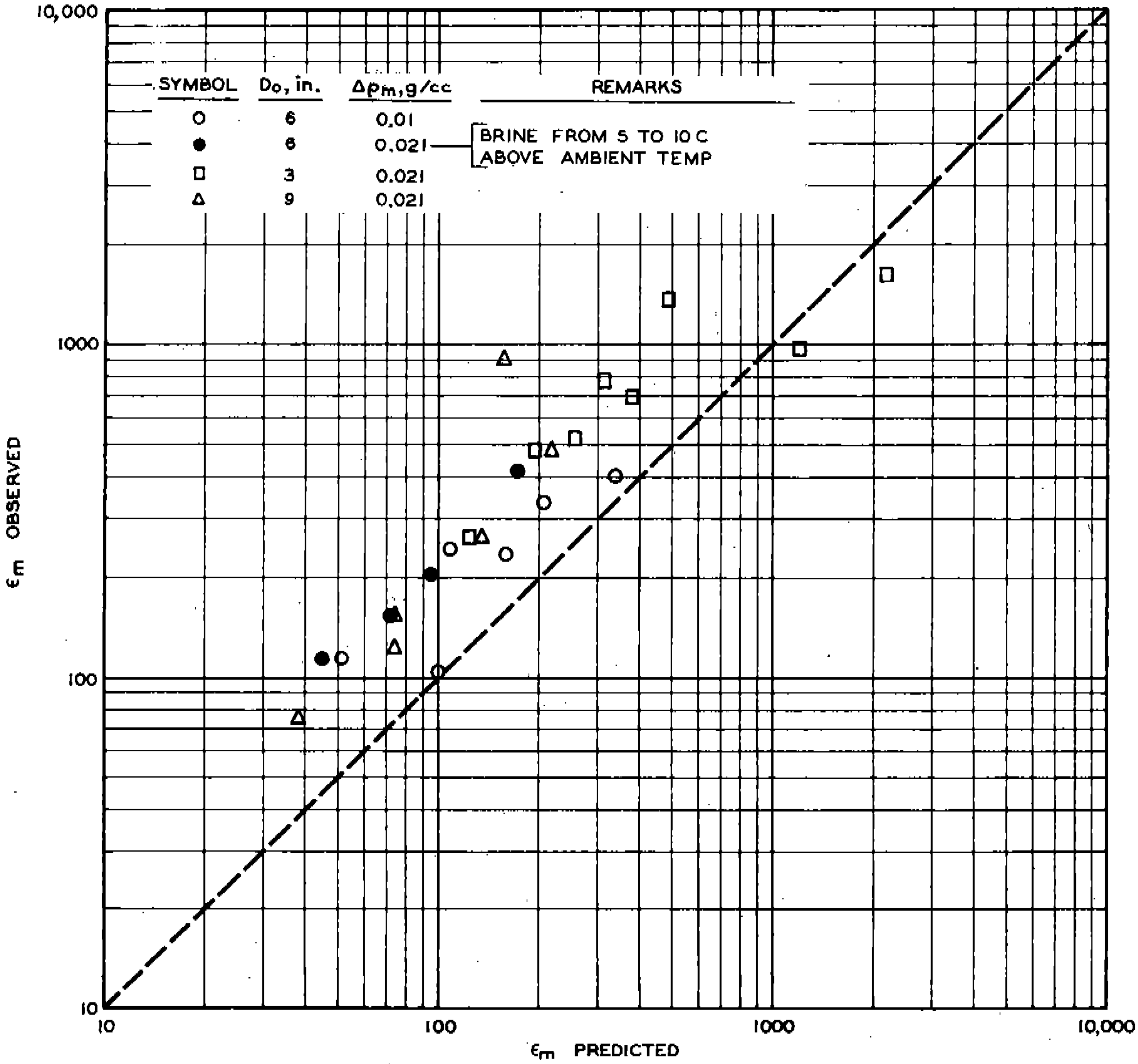

Fig. 16. Vertification of dimensionless dilution correlation, equation 14

do not fall appreciably outside the basic scatter of fig. 9, and the errors in prediction are conservative; that is, predicted dilutions may be too low. (Predicted concentrations may be too high.) This suggests that equation 14 still can be used in designing diffusers for which the concentration at some downstream point is not to exceed a specified maximum.

In developing equation 14, it was noted that, for any given value of $(U/V_o)F_D$, the dilution is proportional to $(x/x_o)^{0.68}$, where the exponent 0.68 is a constant for both $x/x_o \leq 1.0$ and $x/x_o > 1.0$. On the other hand, w/w_o, the dimensionless plume width, was found to increase more rapidly for $x/x_o > 1.0$ than for $x/x_o \leq 1.0$. This apparent contradiction results from the fact that the arcing plume for which $x/x_o \leq 1.0$ is generally round in cross section, and the width w is thus descriptive of the cross-sectional diameter, or area. On the other hand, for $x/x_o > 1.0$, the plume has a more rectangular cross section, and the width w alone does not fully account for the cross-sectional area. Now the entrainment of ambient fluid into the plume, which results in dilution and an increasing cross-sectional area, is governed primarily by the turbulence of the plume and the ambient fluid; therefore, the transition at $x/x_o = 1.0$ from an arcing plume to dense flow on the bottom should not necessarily result in increased dilution or cross-sectional area, even though the rate of lateral spread does increase.

The calculated minimum dilution data for the heated brine test are also plotted on fig. 16. The systematic deviation from the prediction by equation 15 is considered to be due to the inaccurate recording of some experimental parameter, for fig. 14 demonstrates excellent agreement between this test and its nonheated counterpart. Temperature probes indicated that the heated brine reached thermal equilibrium with the ambient flow almost immediately after leaving the port. This would be less true of a jet discharged from a large port, in which a thick, undisturbed potential core would have minimum losses to the ambient fluid. From this limited test it can be tentatively concluded that a temperature differential of up to 10°C between the brine effluent and the ambient fluid will have essentially no effect on the validity of results using nonheated brine.

D. Recommended Application of Results

A primary consideration in designing desalination plant outfall systems is whether the dense plume will reach the surface, desirable for mixing but aesthetically objectionable, or remain submerged, with a decrease in overall mixing but less effect on surface appearance and recreational activity. Equation 4 provides a method of balancing port diameter, number of ports, total brine flow rate, and density differential with the ambient velocity to obtain a desired maximum jet height. Where the ambient velocity varies periodically, as in an estuary, the required rates of diversion of brine to holding tanks can be calculated for acceptable jet performance during slack-water periods.

Although generalized three-dimensional dilution patterns downstream of a diffuser were not developed as part of this study, equation 14 does provide a means of predicting the maximum concentrations of effluent to be expected at some downstream distance from the diffuser. Thus the port diameter, number of ports, total brine flow rate, density differential, and maximum jet height can be balanced with the ambient velocity to meet established water-quality criteria downstream.

Equations 7-11 can be used to predict the lateral spread of dense plumes, which must be done before superposition of single-port results can be accomplished. As part of a proposed extended research effort, a computer program would be developed to compute three-dimensional mixing and geometry characteristics for any set of design and operation conditions, including unsteady ambient flow. Such a program would also compute specific combinations of design and operation parameters that would permit plant operation consistent with specific water-quality criteria.

SECTION VII: LITERATURE CITED

1. Dow Chemical Co., "Conceptual Designs of Outfall Systems for Desalting Plants," Office of Saline Water Research and Development Progress Report No. 550, U. S. Dept. of Interior, Washington, D. C.

2. Keffer, J. F. and Baines, W. D., "The Round Turbulent Jet in a Cross-Wind," Journal of Fluid Mechanics, Vol 15, Part 4, Apr 1963, pp 481-496.

3. Fan, L.-N., "Turbulent Buoyant Jets into Stratified or Flowing Ambient Fluids," Report No. KH-R-15, June 1967, California Institute of Technology, W. M. Keck Laboratory, Pasadena, Calif.

4. Crew, H., "A Numerical Model of the Dispersion of a Dense Effluent in a Stream," A&M Project 716, Reference 70-10T, June 1970, Texas A&M University, Department of Oceanography and Meteorology, College Station, Tex.

5. Turner, J. S., "Jets and Plumes with Negative or Reversing Buoyance," Journal of Fluid Mechanics, Vol 26, Part 4, Dec 1966, pp 779-792.

6. Tilton, L. W. and Taylor, J. K., "Accurate Representation of the Refractivity and Density of Distilled Water as a Function of Temperature," Journal of Research of the National Bureau of Standards, Vol 18, Research Paper RP-971, Feb 1937, pp 205-214.

SECTION VIII: SELECTED BIBLIOGRAPHY

Albertson, M. L., et al., "Diffusion of Submerged Jets," Transactions, American Society of Civil Engineers, Vol 115, 1950, pp 639-664.

Bradbury, L. J. S. and Wood, M. N., "The Static Pressure Distribution Around a Circular Jet Exhausting Normally from a Plane Wall into an Air-Stream," Technical Note No. Aero 2978, Aug 1964, British Royal Aircraft Establishment.

Callaghan, E. E. and Bowden, D. T., "Investigation of the Penetration of an Air Jet Directed Perpendicularly to an Air Stream," TN 1615, June 1948, National Advisory Committee for Aeronautics, Washington, D. C.

Carter, H. H., "A Preliminary Report on the Characteristics of a Heated Jet Discharged Horizontally into a Transverse Current; Part I, Constant Depth," Technical Report No. 61, Reference 69-14, Nov 1969, Johns Hopkins University, Chesapeake Bay Institute, Baltimore, Md.

Gordier, R., "Studies on Fluid Jets Discharging Normally into Moving Fluid," Technical Paper No. 28, Series B, Aug 1959, University of Minnesota, St. Anthony Falls Hydraulic Laboratory, Minneapolis, Minn.

Jordinson, R., "Flow in a Jet Directed Normal to the Wind," R&M 3074, Oct 1956, British Aeronautical Research Council.

Lee, C. C., "A Review of Research on the Interaction of a Jet with an External Stream," Technical Note R-184, Mar 1966, Brown Engineering Co., Inc., Huntsville, Ala.

Lee, S.-L., "Axisymmetrical Turbulent Swirling Natural-Convection Plume," Journal of Applied Mechanics, Vol 33, Series E, No. 3, Sept 1966, pp 647-667.

Liseth, P., "Mixing of Merging Buoyant Jets from a Manifold in Stagnant Receiving Water of Uniform Density," Technical Report HEL 23-1, Nov 1970, University of California at Berkeley, Hydraulic Engineering Laboratory, Berkeley, Calif.

McAllister, J. D., "A Momentum Theory for the Effects of Cross Flow on Impressible Turbulent Jets," Ph. D. dissertation, Aug 1968, University of Tennessee, Knoxville, Tenn.

Mosher, D. K., "An Experimental Investigation of a Turbulent Jet in a Cross Flow," Report 70-7, Dec 1970, Georgia Institute of Technology, School of Aerospace Engineering, Atlanta, Ga.

Pratte, B. C. and Baines, W. D., "Profiles of the Round Turbulent Jet in a Cross Flow," Journal, Hydraulics Division, American Society of Civil Engineers, Vol 93, No. HY6, Nov 1967, pp 53-64.

Pratte, B. C. and Keffer, J. F., "Swirling Turbulent Jet Flows; Part I: The Single Swirling Jet," UTME-TP 6901, Mar 1969, Department of Mechanical Engineering, University of Toronto, Toronto, Canada.

Ruggeri, R., Callaghan, E., and Bowden, D., "Penetration of Air Jets Issuing from Circular, Square, and Elliptical Orifices Directed Perpendicularly to an Air Stream," TN 2019, Feb 1950, National Advisory Committee for Aeronautics, Washington, D. C.

Stolzenbach, K. D. and Harleman, D. R. F., "An Analytical and Experimental Investigation of Surface Discharges of Heated Water," Report No. 135, Feb 1971, Massachusetts Institute of Technology, Ralph M. Parsons Laboratory for Water Resources and Hydrodynamics, Cambridge, Mass.

Wu, J. D., Mosher, D. K., and Wright, M. A., "Experimental and Analytical Investigations of Jets Exhausting into a Deflecting Stream," Journal of Aircraft, Vol 7, No. 1, Jan-Feb 1970.

Table 1

Jet Geometry Tests

Test	D_o in.	D in.	ρ_f g/cc	$\Delta\rho_m$ g/cc	$\mathbb{F}_D$	U knots	H ft	Z_m ft
301	3	20	0.9972	0.0180	18.8	0.10	40	14.4
302	3	20	0.9972	0.0180	24.5	0.10	40	21.0
303	3	20	0.9972	0.0180	29.8	0.10	40	25.6
304	3	20	0.9972	0.0180	35.7	0.10	40	30.0
305	3	20	0.9972	0.0180	41.4	0.10	40	36.0
306	3	20	0.9972	0.0180	46.8	0.10	40	40.0
307	3	20	0.9972	0.0180	18.8	0.21	40	11.0
308	3	20	0.9972	0.0180	24.5	0.21	40	15.6
309	3	20	0.9972	0.0180	29.8	0.21	40	21.8
310	3	20	0.9972	0.0180	35.7	0.21	40	25.5
311	3	20	0.9972	0.0180	41.4	0.21	40	28.8
312	3	20	0.9972	0.0180	46.8	0.21	40	32.2
313	3	20	0.9972	0.0180	52.4	0.21	40	37.0
314	3	20	0.9972	0.0182	18.4	0.31	40	12.9
315	3	20	0.9972	0.0182	24.1	0.31	40	13.6
316	3	20	0.9972	0.0182	29.9	0.31	40	14.9
317	3	20	0.9972	0.0182	35.3	0.31	40	21.0
318	3	20	0.9972	0.0182	41.0	0.31	40	23.1
319	3	20	0.9972	0.0182	46.4	0.31	40	28.3
320	3	20	0.9972	0.0182	51.9	0.31	40	29.1
321	3	20	0.9970	0.0184	18.5	0.44	40	7.9
322	3	20	0.9970	0.0184	24.1	0.44	40	10.3
323	3	20	0.9970	0.0184	29.7	0.44	40	15.1
324	3	20	0.9970	0.0184	35.1	0.44	40	17.0
325	3	20	0.9970	0.0184	41.0	0.44	40	20.4
326	3	20	0.9970	0.0184	46.2	0.44	40	24.2
327	3	20	0.9970	0.0184	52.0	0.44	40	23.3
328	3	20	0.9969	0.0185	18.5	0.48	40	8.7
329	3	20	0.9969	0.0185	24.1	0.48	40	13.1
330	3	20	0.9969	0.0185	29.7	0.48	40	13.6
331	3	20	0.9969	0.0185	35.1	0.48	40	17.2
332	3	20	0.9969	0.0185	41.0	0.48	40	17.5
333	3	20	0.9969	0.0185	46.2	0.48	40	21.2
334	3	20	0.9969	0.0185	52.0	0.48	40	25.9
335	3	20	0.9969	0.0182	18.4	0.75	40	7.5
336	3	20	0.9969	0.0182	24.1	0.75	40	9.2
337	3	20	0.9969	0.0182	29.9	0.75	40	8.8
338	3	20	0.9969	0.0182	35.3	0.74	40	12.0
339	3	20	0.9969	0.0182	41.0	0.75	40	13.0
340	3	20	0.9969	0.0182	46.4	0.75	40	15.9
341	3	20	0.9969	0.0182	51.9	0.75	40	17.8
342	3	20	0.9969	0.0177	18.9	1.00	40	5.6
343	3	20	0.9969	0.0177	24.6	1.00	40	8.8
344	3	20	0.9969	0.0177	30.2	1.00	40	6.9
345	3	20	0.9969	0.0177	35.7	1.00	40	9.2
346	3	20	0.9969	0.0177	41.8	1.00	40	9.8
347	3	20	0.9969	0.0177	47.0	1.00	40	7.5
348	3	20	0.9969	0.0177	52.0	1.00	40	10.0
350	3	20	0.9978	0.0105	25.0	0.10	40	20.7
351	3	20	0.9978	0.0105	40.3	0.10	40	33.1
352	3	20	0.9978	0.0105	55.3	0.10	40	40.0
353	3	20	0.9978	0.0105	70.0	0.10	40	40.0
354	3	20	0.9978	0.0105	25.0	0.31	40	9.8
355	3	20	0.9978	0.0105	40.3	0.31	40	18.8

(Continued) (1 of 7 sheets)

Table 1 (Continued)

Test	D_o in.	D in.	ρ_f g/cc	$\Delta\rho_m$ g/cc	F_D	U knots	H ft	Z_m ft
356	3	20	0.9978	0.0105	55.3	0.31	40	25.0
357	3	20	0.9978	0.0105	70.0	0.31	40	30.2
358	3	20	0.9978	0.0105	25.0	0.50	40	8.5
359	3	20	0.9978	0.0105	40.3	0.50	40	11.4
360	3	20	0.9978	0.0105	55.3	0.50	40	19.0
361	3	20	0.9978	0.0105	70.0	0.50	40	23.0
362	3	20	0.9978	0.0105	25.0	0.75	40	5.0
363	3	20	0.9978	0.0105	40.3	0.75	40	7.0
364	3	20	0.9978	0.0105	55.3	0.75	40	9.0
365	3	20	0.9978	0.0105	70.0	0.75	40	12.0
366	3	20	1.0002	0.0263	15.6	0.10	40	9.8
367	3	20	1.0002	0.0263	25.3	0.10	40	16.8
368	3	20	1.0002	0.0263	34.7	0.10	40	20.5
369	3	20	1.0002	0.0263	44.0	0.10	40	31.0
370	3	20	1.0002	0.0157	20.0	0.10	40	11.2
371	3	20	1.0002	0.0157	32.3	0.10	40	22.7
372	3	20	1.0002	0.0157	44.3	0.10	40	32.8
373	3	20	1.0002	0.0157	56.2	0.10	40	40.0
374	3	20	1.0002	0.0157	20.0	0.30	40	9.0
375	3	20	1.0002	0.0157	32.3	0.30	40	17.0
376	3	20	1.0002	0.0157	44.3	0.30	40	23.0
377	3	20	1.0002	0.0157	56.2	0.30	40	30.2
378	3	20	1.0002	0.0263	15.6	0.30	40	6.7
379	3	20	1.0002	0.0263	25.3	0.30	40	11.0
380	3	20	1.0002	0.0263	34.7	0.30	40	20.0
381	3	20	1.0002	0.0263	44.0	0.30	40	24.0
382	3	20	1.0002	0.0263	15.6	0.50	40	6.2
383	3	20	1.0002	0.0263	25.3	0.50	40	11.5
384	3	20	1.0002	0.0263	34.7	0.50	40	14.4
385	3	20	1.0002	0.0263	44.0	0.50	40	20.0
386	3	20	1.0002	0.0157	20.0	0.50	40	9.6
387	3	20	1.0002	0.0157	32.3	0.50	40	15.0
388	3	20	1.0002	0.0157	44.3	0.50	40	20.2
389	3	20	1.0002	0.0157	56.2	0.50	40	23.4
390	3	20	1.0002	0.0157	20.0	0.75	40	8.6
391	3	20	1.0002	0.0157	32.3	0.75	40	11.2
392	3	20	1.0002	0.0157	44.3	0.75	40	12.0
393	3	20	1.0002	0.0157	56.2	0.75	40	16.0
394	3	20	1.0002	0.0263	15.6	0.75	40	6.8
395	3	20	1.0002	0.0263	25.3	0.75	40	9.0
396	3	20	1.0002	0.0263	34.7	0.75	40	10.0
397	3	20	1.0002	0.0263	44.0	0.75	40	13.0
398	3	20	1.0002	0.0263	15.6	1.00	40	5.0
399	3	20	1.0002	0.0263	25.3	1.00	40	8.5
400	3	20	1.0002	0.0263	34.7	1.00	40	10.0
401	3	20	1.0002	0.0263	44.0	1.00	40	10.3
402	3	20	1.0002	0.0157	20.0	1.00	40	5.2
403	3	20	1.0002	0.0157	32.3	1.00	40	8.6
404	3	20	1.0002	0.0157	44.3	1.00	40	10.0
405	3	20	1.0002	0.0157	56.2	1.00	40	14.2
406	3	20	1.0007	0.0045	37.0	0.10	40	21.2
407	3	20	1.0007	0.0045	58.0	0.10	40	34.0
408	3	20	1.0007	0.0045	79.6	0.10	40	40.0
409	3	20	1.0007	0.0045	37.0	0.30	40	12.0

(Continued) (2 of 7 sheets)

Table 1 (Continued)

Test	D_o in.	D in.	ρ_f g/cc	$\Delta\rho_m$ g/cc	$\mathbb{F}_D$	U knots	H ft	Z_m ft
410	3	20	1.0007	0.0045	58.0	0.30	40	21.3
411	3	20	1.0007	0.0045	79.6	0.30	40	27.2
412	3	20	1.0007	0.0045	100.3	0.30	40	31.6
413	3	20	1.0007	0.0045	37.0	0.50	40	7.8
414	3	20	1.0007	0.0045	58.0	0.50	40	13.7
415	3	20	1.0007	0.0045	79.6	0.50	40	15.8
416	3	20	1.0007	0.0045	100.3	0.50	40	21.0
601	6	10	0.9968	0.0192	12.5	0.10	40	21.2
602	6	10	0.9968	0.0192	15.9	0.10	40	29.5
603	6	10	0.9968	0.0192	20.0	0.10	40	34.5
604	6	10	0.9980	0.0192	24.8	0.10	40	40.0
605	6	10	0.9968	0.0192	27.3	0.10	40	40.0
606	6	10	0.9968	0.0192	29.2	0.10	40	40.0
607	6	10	0.9970	0.0189	12.4	0.32	40	16.6
608	6	10	0.9970	0.0189	16.0	0.32	40	23.6
609	6	10	0.9970	0.0189	24.9	0.32	40	26.5
610	6	10	0.9970	0.0189	29.2	0.32	40	40.0
611	6	10	0.9970	0.0189	13.8	0.50	40	16.2
612	6	10	0.9970	0.0189	20.0	0.50	40	18.0
613	6	10	0.9970	0.0189	27.4	0.50	40	25.1
614	6	10	0.9970	0.0189	34.8	0.50	40	38.2
615	6	20	0.9968	0.0190	13.7	0.10	40	27.6
616	6	20	0.9968	0.0190	17.1	0.10	40	29.2
617	6	20	0.9968	0.0190	19.5	0.10	40	36.1
618	6	20	0.9968	0.0190	22.3	0.10	40	39.3
619	6	20	0.9968	0.0190	25.8	0.10	40	40.0
620	6	20	0.9968	0.0190	28.9	0.10	40	40.0
621	6	20	0.9968	0.0190	33.6	0.10	40	40.0
622	6	20	0.9968	0.0190	37.5	0.10	40	40.0
623	6	20	0.9968	0.0187	13.7	0.21	40	20.0
624	6	20	0.9968	0.0187	17.1	0.21	40	25.8
625	6	20	0.9968	0.0187	19.5	0.21	40	31.2
626	6	20	0.9968	0.0187	22.3	0.21	40	32.9
627	6	20	0.9968	0.0187	25.8	0.21	40	40.0
628	6	20	0.9968	0.0187	28.9	0.21	40	40.0
629	6	20	0.9968	0.0187	33.6	0.21	40	40.0
630	6	20	0.9968	0.0187	37.5	0.21	40	40.0
631	6	20	0.9968	0.0189	13.7	0.31	40	21.2
632	6	20	0.9968	0.0189	17.1	0.31	40	21.8
633	6	20	0.9968	0.0189	19.5	0.31	40	25.3
634	6	20	0.9968	0.0189	22.3	0.31	40	33.8
635	6	20	0.9968	0.0189	25.8	0.31	40	37.9
636	6	20	0.9968	0.0189	28.9	0.31	40	40.0
637	6	20	0.9968	0.0189	33.6	0.31	40	40.0
638	6	20	0.9968	0.0189	37.5	0.31	40	40.0
639	6	20	0.9968	0.0185	13.8	0.44	40	18.0
640	6	20	0.9968	0.0185	17.2	0.44	40	19.6
641	6	20	0.9968	0.0185	19.6	0.44	40	21.8
642	6	20	0.9968	0.0185	22.7	0.44	40	26.1
643	6	20	0.9968	0.0185	26.0	0.44	40	29.8
644	6	20	0.9968	0.0185	29.3	0.44	40	33.8
645	6	20	0.9968	0.0185	34.0	0.44	40	40.0
646	6	20	0.9968	0.0185	37.8	0.44	40	40.0
647	6	20	0.9966	0.0190	13.7	0.48	40	14.3

(Continued)

Table 1 (Continued)

Test	D_o in.	D in.	ρ_f g/cc	$\Delta\rho_m$ g/cc	F_D	U knots	H ft	Z_m ft
648	6	20	0.9966	0.0190	17.1	0.48	40	17.2
649	6	20	0.9966	0.0190	19.5	0.48	40	21.0
650	6	20	0.9966	0.0190	22.3	0.48	40	22.5
651	6	20	0.9966	0.0190	25.8	0.48	40	25.9
652	6	20	0.9966	0.0190	28.9	0.48	40	32.8
653	6	20	0.9966	0.0190	33.6	0.48	40	34.0
654	6	20	0.9966	0.0190	37.5	0.48	40	40.0
655	6	20	0.9968	0.0182	13.9	0.50	40	14.0
656	6	20	0.9968	0.0182	17.3	0.50	40	17.0
657	6	20	0.9968	0.0182	19.9	0.50	40	20.0
658	6	20	0.9968	0.0182	22.8	0.50	40	24.1
659	6	20	0.9968	0.0182	26.2	0.50	40	28.2
660	6	20	0.9968	0.0182	29.5	0.50	40	30.5
661	6	20	0.9968	0.0182	34.1	0.50	40	40.0
662	6	20	0.9968	0.0182	38.1	0.50	40	40.0
663	6	20	0.9965	0.0200	13.3	0.75	40	13.2
664	6	0	0.9965	0.0200	16.7	0.75	40	14.0
665	6	20	0.9965	0.0200	19.0	0.75	40	16.6
666	6	20	0.9965	0.0200	21.7	0.75	40	20.2
667	6	20	0.9965	0.0200	25.0	0.75	40	23.0
668	6	20	0.9965	0.0200	28.1	0.75	40	22.9
669	6	20	0.9965	0.0200	32.7	0.75	40	23.9
670	6	20	0.9965	0.0200	36.3	0.75	40	23.9
671	6	20	0.9965	0.0198	13.3	1.00	40	9.9
672	6	20	0.9965	0.0198	16.7	1.00	40	14.9
673	6	20	0.9965	0.0198	19.0	1.00	40	15.9
674	6	20	0.9965	0.0198	21.7	1.00	40	17.8
675	6	20	0.9965	0.0198	25.0	1.00	40	23.0
676	6	20	0.9965	0.0198	28.1	1.00	40	24.6
677	6	20	0.9965	0.0198	32.7	1.00	40	27.8
678	6	20	0.9965	0.0198	38.3	1.00	40	28.2
680	6	20	0.9983	0.0100	18.4	0.10	40	30.5
681	6	20	0.9983	0.0100	26.3	0.10	40	40.0
682	6	20	0.9983	0.0100	18.4	0.21	40	24.6
683	6	20	0.9983	0.0100	26.3	0.21	40	40.0
684	6	20	0.9983	0.0100	35.2	0.21	40	40.0
685	6	20	0.9983	0.0100	18.4	0.31	40	22.1
686	6	20	0.9983	0.0100	26.3	0.31	40	28.1
687	6	20	0.9983	0.0100	35.2	0.31	40	40.0
688	6	20	0.9983	0.0100	45.8	0.31	40	40.0
689	6	20	0.9983	0.0100	18.4	0.44	40	13.8
690	6	20	0.9983	0.0100	26.3	0.44	40	20.9
691	6	20	0.9983	0.0100	35.2	0.44	40	30.3
692	6	20	0.9983	0.0100	45.8	0.44	40	40.0
693	6	20	0.9983	0.0100	18.4	0.50	40	15.7
694	6	20	0.9983	0.0100	26.3	0.50	40	21.0
695	6	20	0.9983	0.0100	35.2	0.50	40	28.0
696	6	20	0.9983	0.0100	45.8	0.50	40	40.0
697	6	20	0.9983	0.0100	18.4	0.75	40	11.9
698	6	20	0.9983	0.0100	26.3	0.75	40	12.0
699	6	20	0.9983	0.0100	35.2	0.75	40	19.4
700	6	20	0.9983	0.0100	45.8	0.75	40	25.7
701	6	20	0.9983	0.0100	18.4	1.00	40	8.0
702	6	20	0.9983	0.0100	26.3	1.00	40	12.0

(Continued) (4 of 7 sheets)

Table 1 (Continued)

Test	D_o in.	D in.	ρ_f g/cc	$\Delta\rho_m$ g/cc	F_D	U knots	H ft	Z_m ft
703	6	20	0.9983	0.0100	35.2	1.00	40	17.1
704	6	20	0.9983	0.0100	45.8	1.00	40	27.5
705	6	20	1.0002	0.0263	11.4	0.10	40	15.5
706	6	20	1.0002	0.0263	16.4	0.10	40	18.3
707	6	20	1.0002	0.0263	21.7	0.10	40	32.7
708	6	20	1.0002	0.0263	28.3	0.10	40	40.0
709	6	20	1.0020	0.0155	14.9	0.10	40	18.9
710	6	20	1.0020	0.0155	21.5	0.10	40	28.2
711	6	20	1.0020	0.0155	28.5	0.10	40	40.0
712	6	20	1.0002	0.0155	14.9	0.20	40	19.7
713	6	20	1.0002	0.0155	21.5	0.20	40	29.2
714	6	20	1.0002	0.0155	28.5	0.20	40	40.0
715	6	20	1.0002	0.0263	11.4	0.20	40	40.0
716	6	20	1.0002	0.0263	16.4	0.20	40	24.3
717	6	20	1.0002	0.0263	21.7	0.20	40	33.3
718	6	20	1.0002	0.0263	28.3	0.20	40	40.0
719	6	20	1.0002	0.0263	11.4	0.30	40	13.3
720	6	20	1.0002	0.0263	16.4	0.30	40	22.2
721	6	20	1.0002	0.0263	21.7	0.30	40	31.0
722	6	20	1.0002	0.0263	28.3	0.30	40	40.0
723	6	20	1.0002	0.0155	14.9	0.30	40	19.5
724	6	20	1.0002	0.0155	21.5	0.30	40	27.3
725	6	20	1.0002	0.0155	28.5	0.30	40	32.6
726	6	20	1.0002	0.0155	37.0	0.30	40	40.0
727	6	20	1.0002	0.0155	14.9	0.50	40	14.5
728	6	20	1.0002	0.0155	21.5	0.50	40	20.7
729	6	20	1.0002	0.0155	28.5	0.50	40	25.5
730	6	20	1.0002	0.0155	37.0	0.50	40	30.8
731	6	20	1.0002	0.0263	11.4	0.50	40	12.0
732	6	20	1.0002	0.0263	16.4	0.50	40	18.2
733	6	20	1.0002	0.0263	21.7	0.50	40	25.0
734	6	20	1.0002	0.0263	28.3	0.50	40	31.2
735	6	20	1.0002	0.0263	11.4	0.75	40	10.0
736	6	20	1.0002	0.0263	16.4	0.75	40	14.0
737	6	20	1.0002	0.0263	21.7	0.75	40	17.0
738	6	20	1.0002	0.0263	28.3	0.75	40	21.3
739	6	20	1.0002	0.0153	14.9	0.75	40	12.9
740	6	20	1.0002	0.0153	21.5	0.75	40	16.6
741	6	20	1.0002	0.0153	28.5	0.75	40	20.4
742	6	20	1.0002	0.0153	37.0	0.75	40	22.7
743	6	20	1.0002	0.0153	14.9	1.00	40	17.4
744	6	20	1.0002	0.0153	21.5	1.00	40	18.5
745	6	20	1.0002	0.0153	28.5	1.00	40	20.0
746	6	20	1.0002	0.0153	37.0	1.00	40	21.5
747	6	20	1.0002	0.0263	11.4	1.00	40	9.6
748	6	20	1.0002	0.0263	16.4	1.00	40	14.5
749	6	20	1.0002	0.0263	21.7	1.00	40	18.5
750	6	20	1.0002	0.0263	28.3	1.00	40	21.6
751	6	20	1.0005	0.0046	25.5	0.10	40	40.0
752	6	20	1.0005	0.0046	38.3	0.10	40	40.0
753	6	20	1.0005	0.0046	26.5	0.30	40	20.0
754	6	20	1.0005	0.0046	38.3	0.30	40	30.3
755	6	20	1.0005	0.0046	50.8	0.30	40	40.0
756	6	20	1.0005	0.0046	65.7	0.30	40	40.0

(Continued) (5 of 7 sheets)

Table 1 (Continued)

Test	D_o in.	D in.	ρ_f g/cc	$\Delta\rho_m$ g/cc	$\mathbb{F}_D$	U knots	H ft	Z_m ft
757	6	20	1.0005	0.0046	26.5	0.50	40	18.6
758	6	20	1.0005	0.0046	38.3	0.50	40	19.8
759	6	20	1.0005	0.0046	50.8	0.50	40	28.6
760	6	20	1.0005	0.0046	65.7	0.50	40	30.8
761	6	20	1.0005	0.0046	26.5	0.75	40	12.2
762	6	20	1.0005	0.0046	38.3	0.75	40	15.0
763	6	20	1.0005	0.0046	50.8	0.75	40	20.2
764	6	20	1.0005	0.0046	65.7	0.75	40	23.0
765	6	20	1.0005	0.0046	26.5	1.00	40	11.3
766	6	20	1.0005	0.0046	50.8	1.00	40	16.4
901	9	30	0.9967	0.0198	11.9	0.10	40	33.1
902	9	30	0.9967	0.0198	15.1	0.10	40	40.0
903	9	30	0.9967	0.0198	18.0	0.10	40	40.0
904	9	30	0.9967	0.0198	21.1	0.10	40	40.0
905	9	30	0.9967	0.0198	23.5	0.10	40	40.0
906	9	30	0.9967	0.0198	26.4	0.10	40	40.0
907	9	30	0.9967	0.0198	29.0	0.10	40	40.0
908	9	30	0.9967	0.0196	11.9	0.21	40	31.0
909	9	30	0.9967	0.0196	15.1	0.21	40	37.3
910	9	30	0.9967	0.0196	18.0	0.21	40	40.0
911	9	30	0.9967	0.0196	21.1	0.21	40	40.0
912	9	30	0.9967	0.0196	23.5	0.21	40	40.0
913	9	30	0.9967	0.0196	26.4	0.21	40	40.0
914	9	30	0.9967	0.0196	29.0	0.21	40	40.0
915	9	30	0.9967	0.0196	11.9	0.31	40	29.8
916	9	30	0.9967	0.0196	15.1	0.31	40	37.8
917	9	30	0.9967	0.0196	18.0	0.31	40	40.0
918	9	30	0.9967	0.0196	21.1	0.31	40	40.0
919	9	30	0.9967	0.0196	23.5	0.31	40	40.0
920	9	30	0.9967	0.0196	26.4	0.31	40	40.0
921	9	30	0.9967	0.0196	29.0	0.31	40	40.0
922	9	30	0.9963	0.0203	11.8	0.44	40	26.0
923	9	30	0.9963	0.0203	15.0	0.44	40	29.7
924	9	30	0.9963	0.0203	17.9	0.44	40	38.8
925	9	30	0.9963	0.0203	21.0	0.44	40	40.0
926	9	30	0.9963	0.0203	23.3	0.44	40	40.0
927	9	30	0.9963	0.0203	26.2	0.44	40	40.0
928	9	30	0.9963	0.0203	28.7	0.44	40	40.0
930	9	30	0.9966	0.0199	11.9	0.48	40	24.6
931	9	30	0.9966	0.0199	15.1	0.48	40	28.2
932	9	30	0.9966	0.0199	18.0	0.48	40	35.0
933	9	30	0.9966	0.0199	21.1	0.48	40	40.0
934	9	30	0.9966	0.0199	23.5	0.48	40	40.0
935	9	30	0.9966	0.0199	26.4	0.48	40	40.0
936	9	30	0.9966	0.0199	29.0	0.48	40	40.0
937	9	30	0.9967	0.0197	11.9	0.50	40	25.1
938	9	30	0.9967	0.0197	15.1	0.50	40	29.9
939	9	30	0.9967	0.0197	18.0	0.50	40	36.2
940	9	30	0.9967	0.0197	21.1	0.50	40	40.0
941	9	30	0.9967	0.0197	23.5	0.50	40	40.0
942	9	30	0.9997	0.0197	26.4	0.50	40	40.0
943	9	30	0.9967	0.0197	29.0	0.50	40	40.0
944	9	30	0.9968	0.0196	11.9	0.75	40	21.1
945	9	30	0.9968	0.0196	15.1	0.75	40	22.0

(Continued) (6 of 7 sheets)

Table 1 (Concluded)

Test	D_o in.	D in.	ρ_f g/cc	$\Delta\rho_m$ g/cc	F_D	U knots	H ft	Z_m ft
946	9	30	0.9968	0.0196	18.0	0.75	40	26.7
947	9	30	0.9968	0.0196	21.1	0.75	40	28.0
948	9	30	0.9968	0.0196	23.5	0.75	40	30.3
949	9	30	0.9968	0.0196	26.4	0.75	40	32.8
950	9	30	0.9968	0.0196	29.0	0.75	40	40.0
951	9	30	0.9967	0.0197	11.9	1.00	40	17.8
952	9	30	0.9967	0.0197	15.1	1.00	40	22.0
953	9	30	0.9967	0.0197	18.0	1.00	40	23.0
954	9	30	0.9967	0.0197	21.1	1.00	40	27.0
955	9	30	0.9967	0.0197	23.5	1.00	40	27.2
956	9	30	0.9967	0.0197	26.4	1.00	40	32.3
957	9	30	0.9967	0.0197	29.0	1.00	40	37.0
960	9	30	0.9983	0.0100	16.6	0.10	40	40.0
961	9	30	0.9983	0.0100	16.6	0.31	40	33.0
962	9	30	0.9983	0.0100	25.2	0.31	40	40.0
963	9	30	0.9983	0.0100	16.6	0.50	40	23.0
964	9	30	0.9983	0.0100	25.2	0.50	40	40.0
965	9	30	0.9983	0.0100	33.0	0.50	40	40.0
966	9	30	0.9983	0.0100	40.8	0.50	40	40.0
967	9	30	0.9983	0.0100	16.6	0.75	40	22.0
968	9	30	0.9983	0.0100	25.2	0.75	40	22.0
969	9	30	0.9983	0.0100	33.0	0.75	40	31.0
970	9	30	0.9983	0.0100	40.8	0.75	40	40.0
971	9	30	0.9982	0.0103	16.6	1.00	40	20.0
972	9	30	0.9982	0.0103	25.2	1.00	40	25.3
973	9	30	0.9982	0.0103	33.0	1.00	40	27.6
974	9	30	0.9982	0.0103	40.8	1.00	40	36.2
975	9	30	0.9982	0.0103	16.6	0.75	30	22.0
976	9	30	0.9982	0.0103	25.2	0.75	30	29.0
977	9	30	0.9982	0.0103	21.1	0.75	30	22.0
978	9	30	0.9982	0.0103	16.6	0.50	30	25.8
979	9	30	0.9982	0.0103	21.1	0.50	30	30.0
980	9	30	0.9982	0.0103	16.6	0.50	30	30.0

(7 of 7 sheets)

Table 2

Dilution Tests

Test	D_o in.	D in.	$\Delta\rho_m$ g/cc	F_D	U knots	H ft	Minimum Observed Dilution (Dimensionless) at Indicated Distance Downstream from Diffuser (ft) 5	10	15	20	30	40	50	60	80	100	120	160	200	220	240	280	320	400	440	480	500
420	3	20	0.021	36.3	0.5	40						262			489		532	792	703				1380				
421	3	20	0.022	36.3	1.0	40									980				1619				3388				
615	6	20	0.021	13.1	0.1	40	40	80	95																		
617	6	20	0.021	18.9	0.1	40		37		63	108																
619	6	20	0.021	25.0	0.1	40		36		49	48	83															
621	6	20	0.021	32.2	0.1	40		37			37		75		103												
623	6	20	0.021	13.2	0.2	40		64			83		108														
625	6	20	0.021	18.3	0.2	40				42		78		81													
627	6	20	0.021	25.1	0.2	40				21		44			55												
629	6	20	0.021	32.6	0.2	40				20				41		68											
631	6	20	0.021	13.0	0.3	40						64			124		190	215									
633	6	20	0.021	19.0	0.3	40						56			85		95	153									
635	6	20	0.021	25.2	0.3	40						66			87		137	131			197						
637	6	20	0.021	32.9	0.3	40						77			102		158	160			200						
639	6	20	0.021	13.2	0.44	40						70				142		156									
641	6	20	0.021	19.0	0.44	40						72				148		182									
643	6	20	0.021	24.7	0.44	40						40				59		78									
645	6	20	0.021	32.7	0.44	40						44				75		86		90							
655	6	20	0.021	13.3	0.5	40						80			124		121	215	182		212						
657	6	20	0.021	18.7	0.5	40						71			148		138	134	177			188					
659	6	20	0.021	24.6	0.5	40						85			172		132	148	170		168						
661	6	20	0.021	32.1	0.5	40						64			115		94	137			177			358			
663	6	20	0.021	13.1	0.75	40						157			197		219	285	426		436	442					
665	6	20	0.021	18.6	0.75	40						125			240			302			408		460		660		
667	6	20	0.021	24.2	0.75	40						128			143			209			387		460		542		603
669	6	20	0.021	31.7	0.75	40						95			178			218			296		396	396			572
671	6	20	0.021	12.9	1.0	40						337			365			680			1060		1020	2000			
673	6	20	0.021	18.3	1.0	40						250			365			570			840		1170	1420			
675	6	20	0.021	24.6	1.0	40						237			382			570			715		900		1520		
677	6	20	0.021	32.1	1.0	40						178			363			700			940		980			1780	
686	6	20	0.011	26.8	0.3	40						116					241										
694	6	20	0.011	26.8	0.5	40						105			238		336				401						
936	9	30	0.021	11.5	0.5	40						76				124		207					909				
950	9	30	0.022	11.5	1.0	40												264					490				
4-615*	6	20	0.021	13.1	0.1	40	33																				
4-655*	6	20	0.021	13.1	0.5	40						150						111									
4-659*	6	20	0.021	24.8	0.5	40						81						128									
4-671*	6	20	0.021	13.1	1.0	40									207							348					
4-675*	6	20	0.021	24.8	1.0	40									184							231					
Heated**	6	20	0.021	18.8	0.5	40						113			157		210					422					
Outfall 1†	--	20	0.021	--	0.1	40																					
Outfall 2†	--	20	0.021	--	0.5	40																					
Outfall 3†	--	20	0.021	--	1.0	40																					

* 4 ports at 13 ft o.c.

** Heated brine.

† Q_b = 5.91 cfs.

Table 3

Lateral Spread Coordinates

Test	Coordinates of Lateral Spread of Brine, ft																	
	x	w	x	w	x	w	x	w	x	w	x	w	x	w	x	w	x	w
307	40	33	80	82	100	103												
308	40	30	80	72	120	106												
309	40	26	80	52	120	91	140	112										
310	40	23	80	48	120	86	60	32	150	113								
311	40	15	80	38	120	106												
312	20	22	80	36	120	76	140	104										
313	40	25	80	23	120	40	155	101										
314	40	20	60	33	80	38	100	47	140	64	180	87						
315	40	11	60	23	80	36	100	50	140	71	180	87						
316	40	15	60	25	80	47	100	57	140	73	180	97						
317	40	17	60	20	80	23	100	31	140	70	180	87						
318	40	16	60	22	80	27	100	32	140	52	180	78	220	97	260	107		
319	46	25	60	29	80	35	100	37	140	49	180	76	220	98				
320	40	23	60	30	80	37	100	38	140	41	180	62	220	96				
321	40	8	80	26	120	32	160	35	200	42	240	54	280	62				
322	40	14	80	24	120	25	160	44	200	49	240	51	280	60	320	65		
323	40	16	80	20	120	27	160	35	200	48	240	70	280	72	320	75		
324	40	17	80	19	120	36	160	36	200	42	240	60	280	67	320	80		
325	40	16	80	25	120	30	160	29	200	49	240	60	280	66	320	72		
326	40	19	80	21	120	26	160	35	200	40	240	53	280	65	320	80		
327	40	20	80	29	120	28	160	33	200	44	240	41	280	59	320	72		
328	40	9	80	27	120	28	160	25	200	23	240	30	280	40	320	44		
329	40	12	80	21	120	28	160	36	200	36	240	49	280	49	320	54		
330	40	10	80	24	120	24	160	34	200	41	240	46	280	60	320	60		
331	40	19	80	23	120	26	160	29	200	25	240	46	280	48	320	72		
333	40	17	80	25	120	33	160	37	200	43	240	48	280	57	320	64		
334	40	18	80	21	120	25	160	34	200	51	240	48	280	48	320	52		
335	40	6	80	7	120	13	160	15	120	24	240	23						
336	40	7	80	10	120	20	160	19	200	16	240	22	280	40				
337	40	9	80	18	120	28	160	25	200	25	240	35	280	37				
338	40	6	80	8	120	13	160	15	200	19	240	20	280	23				
339	40	12	80	22	120	25	160	30	200	30	240	34	280	35	320	40		
340	40	11	80	16	120	24	160	29	200	31	240	33	280	35	320	32		
341	40	15	80	17	120	29	160	31	200	33	240	34	280	40	320	44		
342	40	8	80	12	120	18	160	20	200	18	240	17	280	20				
343	40	8	80	11	120	17	160	22	200	24	240	31						
344	40	8	80	13	120	24	160	21	200	21								
345	40	10	80	14	120	25	160	27	200	25								
346	40	11	80	13	120	15	160	21	200	23	240	20	280	22				
347	40	15	80	23	120	35	160	35	200	36								
348	40	15	80	20	120	25	160	33	200	32								
355	40	17	80	24	120	30												
356	40	18	80	26	120	30												
357	40	24	80	26	120	24												
358	40	12	80	14	120	17												
359	40	17	80	24	120	27												
360	40	19	80	22	120	27												
362	40	12	80	18														
363	40	15	80	23														
364	40	17	80	21	120	27												
623	40	59	60	110														
624	40	59	60	110														
625	40	20	70	114														
626	40	19	70	100														

(Continued) (1 of 4 sheets)

Table 3 (Continued)

Test	Coordinates of Lateral Spread of Brine, ft																	
	x	w	x	w	x	w	x	w	x	w	x	w	x	w	x	w	x	w
627	40	20	80	25	100	118												
628	40	36	80	38	120	118												
631	40	20	60	26														
632	40	19	60	33	80	62												
633	40	32	60	45	80	61	100	71	140	104								
634	40	23	60	28	80	35	100	59	140	105								
635	40	24	60	31	80	36	100	55	140	95	160	109						
636	40	28	60	33	80	34	100	32	140	54	180	95						
637	40	28	60	28	80	30	100	27	140	50	180	93						
638	40	31	60	39	80	42	100	38	140	50	180	70	220	96				
639	40	17	80	27	120	62	160	86										
640	40	20	80	26	120	60	160	82	200	97								
641	40	16	80	30	120	52	160	87	200	102								
642	40	15	80	27	120	53	160	78	200	94								
643	40	17	80	26	120	51	160	74	200	95								
644	40	20	80	26	120	47	160	76	200	91								
645	40	22	80	33	120	40	160	47	200	77	230	92						
646	40	14	80	22	120	33	160	54	200	73	240	97						
647	40	18	80	27	120	53	160	68	200	87	240	100						
648	40	17	80	26	120	45	160	63	200	91								
649	40	11	80	25	120	49	160	65	200	82	240	99						
650	40	17	80	28	120	45	160	65	200	75	240	92						
651	40	24	80	27	120	50	160	57	200	82								
652	40	26	80	30	120	33	160	50	200	74	240	90						
653	40	23	80	36	120	42	160	60	200	78	240	84						
654	40	30	80	36	120	42	160	46	200	60	240	70	280	84				
655	40	17	60	20	80	30	100	43	140	56	180	65	220	80				
656	40	18	60	21	80	26	100	33	140	50	180	70	220	85				
657	40	21	60	23	80	26	100	36	140	56	180	70	220	81				
658	40	21	60	25	80	30	100	35	140	50	180	64	220	80				
659	40	26	60	29	80	30	100	35	140	46	180	70	220	83				
660	40	25	60	30	80	34	100	35	140	42	180	57	220	75	260	90		
661	40	21	60	24	80	28	100	36	140	51	180	60	220	74				
662	40	26	60	29	80	29	100	28	140	34	180	49	220	63	260	72	300	92
663	40	17	60	24	80	26	100	32	140	40	180	45	220	47	260	55	300	65
664	40	19	60	22	80	26	100	26	140	28	180	34	220	40	260	45	300	48
665	40	23	60	22	80	25	100	27	140	34	180	43	220	53	260	65	300	70
666	40	25	60	26	80	27	100	32	140	36	180	43	220	52	260	58	300	67
667	40	15	60	19	80	25	100	29	140	42	180	49	220	51	260	53	300	65
668	40	20	60	21	80	26	100	34	140	42	180	46	220	52	260	55	300	63
669	40	20	60	23	80	27	100	29	140	34	180	44	220	56	260	60	300	69
670	40	19	60	23	80	27	100	28	140	35	180	44	220	46	260	48	300	62
671	40	12	80	17	120	22	160	22	200	24	240	27	280	26	320	28		
672	40	14	80	17	120	21	160	25	200	30	240	30	280	35	320	33		
673	40	21	80	28	120	33	160	39	200	41	240	41	280	40	320	42		
674	40	15	80	22	120	30	160	38	200	40	240	39	280	40	320	40		
675	40	10	80	15	120	22	160	31	200	41	240	44	280	47				
676	40	13	80	20	120	30	160	45	200	46	240	55	280	58	320	60		
677	40	23	80	37	120	42	160	42	200	46	240	49	280	53	320	50		
678	40	16	80	24	120	30	160	36	200	40	240	38	280	37	320	38		
682	40	29	80	67	120	111												
683	40	22	80	33	120	78	140	98										
684	40	32	80	37	120	45	160	67	200	110	225	125						
685	40	21	80	32	120	56	160	85										

(Continued)

(2 of 4 sheets)

Test	Coordinates of Lateral Spread of Brine, ft																	
	x	w	x	w	x	w	x	w	x	w	x	w	x	w	x	w	x	w
686	40	19	80	28	120	54	160	80										
687	40	20	80	27	120	32	160	46	200	86								
688	40	27	80	40	120	45	160	49	200	63								
689	40	20	80	26	120	38	160	52	200	65	240	81						
690	40	19	80	27	120	35	160	54	240	75								
691	40	17	80	26	120	30	160	53	200	67	240	86						
692	40	21	80	37	120	39	160	40	200	42	240	44	280	47	320	57		
693	40	18	80	26	120	37	160	47	200	58	240	67	280	76				
694	40	18	80	26	120	37	160	56	200	70	240	81						
695	40	23	80	33	120	37	160	48	200	58	240	72	280	82				
696	40	24	80	29	120	28	160	31	200	35	240	40	280	44				
697	40	13	80	20	120	22	160	27	200	32	240	39	280	45				
698	40	18	80	27	120	30	160	34	200	37	240	47	280	54	320	56		
699	40	15	80	24	120	27	160	27	200	34	240	45	280	52	320	51		
700	40	19	80	30	120	31	160	36	200	40	240	47	280	52	320	53		
701	40	15	80	23	120	25												
702	40	18	80	25	120	28	160	26	200	26								
703	40	13	80	19	120	23												
704	40	21	80	26	120	25	160	30	200	34	240	36	280	38				
909	40	20																
910	40	20																
915	40	28	60	50	80	90												
916	40	24	60	46	80	73												
917	40	29	60	29	80	34												
918	40	39	60	40	80	42	100	49	120	68	140	98	160	132				
922	40	23	80	38	120	63	160	102										
923	40	16	80	26	120	63	160	64	185	104								
924	40	18	80	26	120	36	160	70	200	96								
925	40	20	80	35	120	40	160	63	200	95	240	116						
926	40	29	80	39	120	40	160	45	200	70	240	101						
927	40	39	80	43	120	47	160	49	200	70	240	99	280	119				
928	40	46	80	64	120	80	160	78	200	83	240	114						
930	40	21	80	30	120	56	160	74	200	93								
931	40	22	80	26	120	36	160	66	200	83								
932	40	20	80	32	120	38	160	56	200	75	240	96						
933	40	18	80	35	120	37	160	43	200	67	240	80	280	96				
934	40	33	80	45	120	45	160	47	200	68	240	69	280	101				
935	40	32	80	48	120	48	160	49	200	67	240	95	280	112				
936	60	29	80	31	100	45	140	66	180	91								
937	60	25	80	30	100	36	140	61	180	82								
938	60	25	80	28	100	30	140	41	180	59	220	80						
939	60	26	80	28	100	27	140	39	180	66	220	91						
940	60	32	80	37	100	39	140	39	180	49	220	72	260	85	300	101		
941	60	36	80	40	100	41	140	43	180	48	220	62	260	88				
942	60	36	80	42	100	46	140	55	180	71	220	80	260	80	300	82		
943	40	19	60	24	80	25	100	32	140	32	180	42	220	54	260	63	300	67
944	40	23	60	26	80	26	100	27	140	36	180	57	220	68	260	73	300	77
945	40	21	60	26	80	31	100	33	140	43	180	56	220	69	260	78	300	83
946	40	19	60	24	80	28	100	31	140	38	180	53	220	63	260	71	300	82
947	40	24	60	27	80	30	100	33	140	50	180	58	220	69	260	78	300	88
948	40	25	60	32	80	37	100	37	140	40	180	44	220	48	260	62	300	87
949	40	26	60	32	80	37	100	40	140	45	180	45	220	45	260	43	300	49
950	40	17	80	22	120	24	160	30	200	38	240	47	280	51	320	54		
951	40	12	80	17	120	25	160	36	200	45	240	43	280	46	320	48		

(Continued)

Table 3 (Concluded)

Test	Coordinates of Lateral Spread of Brine, ft																	
	x	w	x	w	x	w	x	w	x	w	x	w	x	w	x	w	x	w
952	40	25	80	29	120	32	160	42	200	48	240	50	280	50				
953	40	23	80	31	120	35	160	38	200	41	240	42	280	42	320	39		
954	40	24	80	28	120	40	160	32	200	47	240	45	280	47	320	47		
955	40	26	80	33	120	33	160	38	200	42	240	43	280	45	320	47		
956	40	21	80	35	120	33	160	36	200	36	240	38	280	44	320	47		
961	40	19	80	30	120	47	160	81										
962	40	35	80	40	120	40	160	43										
963	40	16	80	25	120	40	160	60	200	73								
964	40	23	80	31	120	35	160	43	200	63	240	82						
965	40	25	80	31	120	37	160	45	200	49	240	53	280	52				
966	40	29	80	41	120	56	160	67	200	73	240	77	280	76				
967	40	16	80	25	120	34	160	42	200	46								
968	40	20	80	28	120	41	160	42	200	45	240	51						
969	40	22	80	27	120	28	160	33	200	40	240	51						
970	40	18	80	34	120	40	160	40	200	43	240	50	280	55				
971	40	13	80	19	120	23	160	30										
972	40	21	80	26	120	29	160	28	200	34	240	40	280	45				
973	40	24	80	25	120	32	160	34	200	40	240	45	280	50	320	53		
974	40	20	80	24	180	27	160	34	200	48	240	57	280	54				
975	40	18	80	22	120	25	160	35	200	39	240	42	280	41				
976	40	19	80	25	120	29	160	38	200	39	240	41	280	42				
977	40	17	80	22	120	24	160	29	200	31	240	37	280	42				
978	40	19	80	24	120	30	160	33	200	43	240	65	280	70				
979	40	22	80	28	120	28	160	30	200	36	240	50	280	53	320	55		

(4 of 4 sheets)

APPENDIX A: NOTATION

A_o	Cross-sectional area of outfall, ft^2
A_p	Cross-sectional area of port, ft^2
B	Dimensionless intercept
B_{T_2}	Calibration intercept at temperature T_2, g/cc
B_{T_3}	Calibration intercept at temperature T_3, g/cc
C	Dimensionless coefficient
C_o	Conductivity meter voltage for a salt solution, mv
D	Outfall diameter, ft or in.
D_o	Port diameter, ft or in.
$\mathbb{F}_D$	Densimetric port Froude number, $V_o \Big/ \sqrt{\dfrac{\Delta\rho_m}{\rho_f} g D_o}$
g	Gravitational acceleration, ft/sec^2
H	Ambient flow depth, ft
Q_b	Brine discharge, cfs
R	Exponent, see equation 9
$\mathbb{R}_c$	Channel Reynolds number
$\mathbb{R}_p$	Port Reynolds number
T	Temperature, C
T_a, T_b	Temperatures of brine solutions, C
T_1	Temperature when solution densities are checked, C
T_2	Temperature when probes are calibrated, C
T_3	Temperature at which data are taken, C
U	Ambient flow velocity, fps
V_o	Average port velocity, fps
w	Plume width, ft
w_o	Total plume width at x_o, ft
x	Distance downstream from port center line, ft
x_o	Downstream distance from port at which plume falls to bottom, ft
y	Distance parallel to diffuser in reference to center of a given port, ft
z	Elevation above bottom, ft

Z_m	Maximum height of upper boundary of jet above bottom, ft
$\Delta\rho$	Far-field effluent density minus ambient fluid density, g/cc
$\Delta\rho_m$	Initial effluent density minus ambient fluid density, g/cc
ϵ	$\Delta\rho_m/\Delta\rho$ = dilution
ϵ_m	Minimum observed dilution
ν	Kinematic viscosity of water, ft^2/sec
ρ	Density, g/cc
ρ_a, ρ_b	Densities of brine solutions, g/cc
ρ_f	Ambient fluid density, g/cc
ρ_{s1}	Solution density at temperature T_1, g/cc
ρ_{s2}	Solution density at temperature T_2, g/cc
ρ_1, ρ_2, ρ_3	Densities of distilled water at temperatures T_1, T_2, T_3, g/cc
ϕ	Indicates functional relation

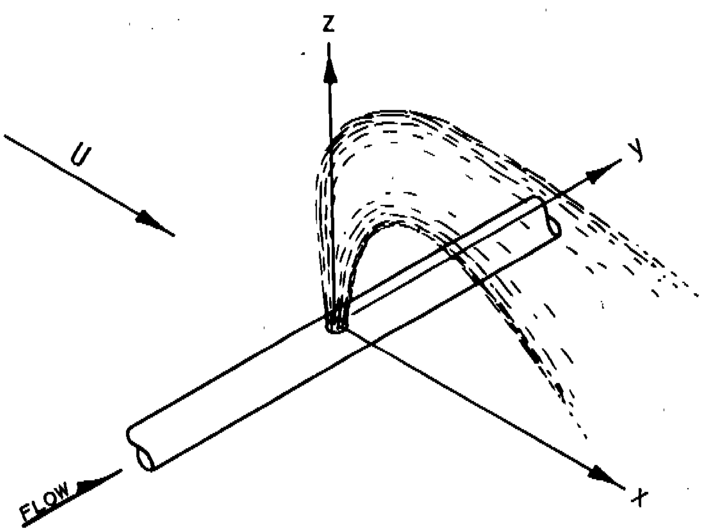

Definition of coordinate system

APPENDIX B: CONDUCTIVITY PROBE CALIBRATION AND DATA REDUCTION

Density is assumed to vary as a function of temperature and salinity only, and conductivity is assumed to vary only with salinity over the small range of temperatures encountered in the testing. At a given temperature, density varies linearly with conductivity (salinity); and at a different temperature, the linear variation has the same slope but is displaced by the difference in the density of distilled water at the two temperatures. An equivalent statement is that the nonlinear temperature-density relation for distilled water is linearly displaced upward by small changes in density due to salinity. Fig. B1 illustrates these relations.

In practice, the temperature of the calibrating solutions differed from one to another; the temperature at which the solutions were checked for density was different from that at which the probes were calibrated; and temperatures during actual testing were still different. In a FORTRAN program written to reduce the calibrations and compute dilutions, the following equation for the density of distilled water is used to make temperature adjustments:[6*]

$$\rho = 1 - \left[\frac{(T - 3.9863)^2}{508{,}929.2} \cdot \frac{T + 288.9414}{T + 68.12963}\right] \tag{B1}$$

where

ρ = density, g/cc

T = temperature, C

Letting

ρ_{s1} = solution density at temperature T_1

ρ_{s2} = solution density at temperature T_2

ρ_1 = density of distilled water at temperature T_1

ρ_2 = density of distilled water at temperature T_2

T_1 = temperature when solution densities are checked

T_2 = temperature when probes are calibrated

the solution densities are converted to density at the calibration temperature by the following equation:

---

* See Literature Cited at end of main text, p 38.

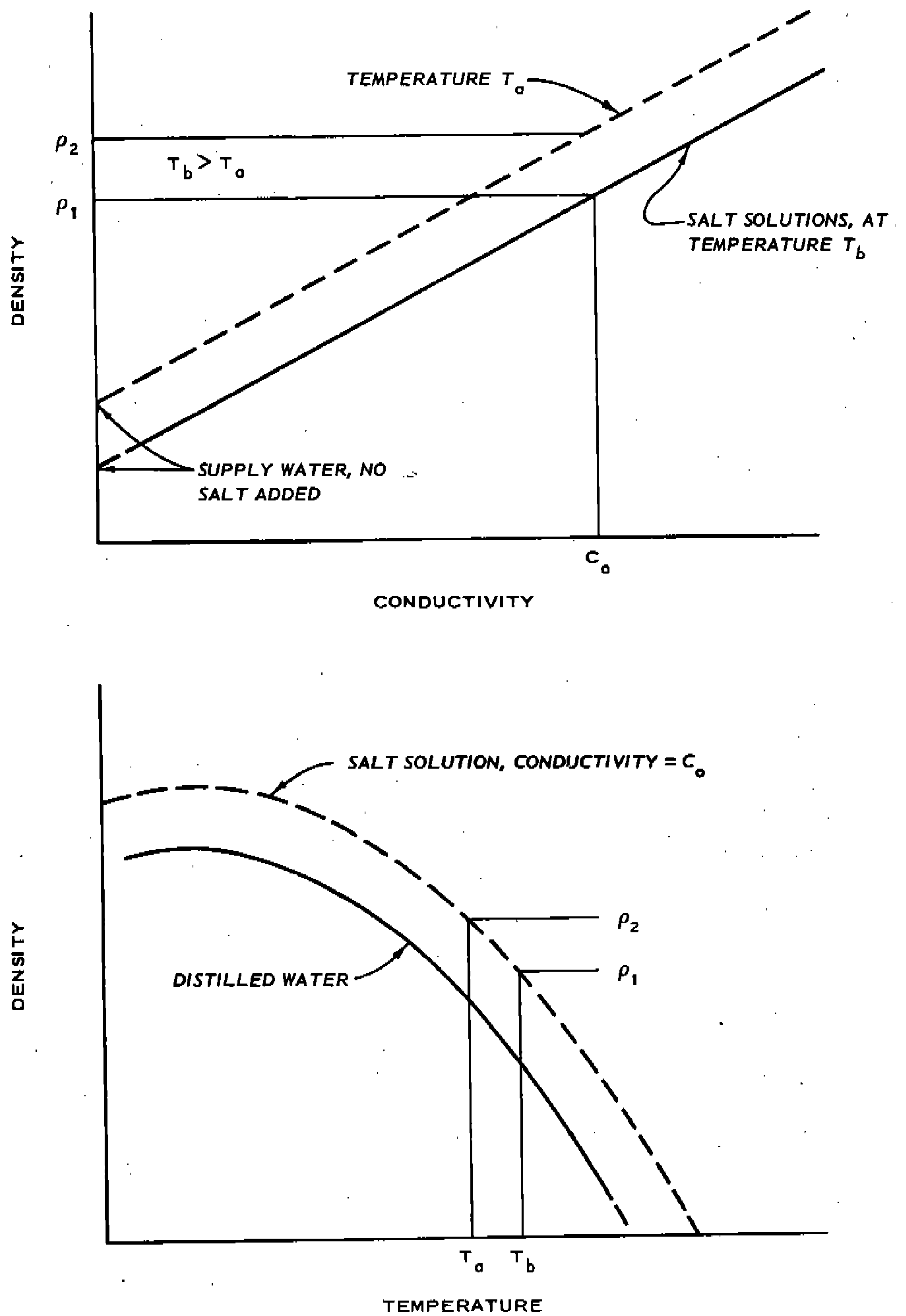

Fig. B1. Conductivity-temperature-density relations

$$\rho_{s2} = \rho_{s1} + (\rho_1 - \rho_2) \tag{B2}$$

At the calibration temperature T_2, linear calibrations of density versus conductivity can be constructed for each probe. A least-squares slope is computed and the intercept calculated by forcing the calibration to pass through the first calibration point, which in practice was "fresh" water; this procedure was necessary to ensure that calibration error was minimized at the sensitive lower ranges of conductivity. These intercepts, representing the density of water having zero conductivity (but denser than distilled water due to suspended solids, etc.), are functions only of temperature. Thus the calibrations of temperature T_2 are adjusted to temperature T_3 by

$$B_{T_3} = B_{T_2} + (\rho_2 - \rho_3) \tag{B3}$$

where

B_{T_2} = calibration intercept at temperature T_2

B_{T_3} = calibration intercept at temperature T_3

ρ_3 = density of distilled water at temperature T_3

T_3 = temperature at which data are taken

In reducing the raw data, the FORTRAN program first processes the calibration data as described above to yield basic linear calibrations. The raw data input consists of grouped conductivities and temperatures, along with a "background" conductivity that represents the approximate freshwater conductivity during the test for each probe. Although the density of the background remains essentially constant at a given temperature, its conductivity may shift slightly from its calibration value due to small changes in background salinity. Therefore, each conductivity reading is slightly adjusted by an amount equal to the background shift between the time of calibration and time of test so that calibrations are continuously updated.

For a given data point, the calibration for that probe is shifted to the data temperature T_3, and a density is computed. In computing dilution, the initial density difference $\Delta\rho_m$ is calculated from hydrometer readings for the brine and ambient fluid, adjusted to the same temperature. The diluted density difference $\Delta\rho$ is the difference between the density as computed from the temperature-conductivity data and the density of the ambient fluid, adjusted to the data temperature. Dilution is then calculated by

$$\epsilon = \frac{\Delta\rho_m}{\Delta\rho} \tag{B4}$$

* U.S. GOVERNMENT PRINTING OFFICE: 1971-444-096/349